Electronic Thesis and Dissertation Repository

8-7-2019 10:00 AM

Development of Cellulose Nanofiber Reinforced Poly(Methyl Methacrylate)

Tyler Bennett, *The University of Western Ontario*

A thesis submitted in partial fulfillment of the requirements for the Master of Engineering Science degree in Mechanical and Materials Engineering

© Tyler Bennett 2019

Follow this and additional works at: https://ir.lib.uwo.ca/etd

Part of the Polymer and Organic Materials Commons

Recommended Citation

Abstract

Cellulose nanofiber (CNF), derived from renewable resources, is a good candidate to reinforce transparent plastics without sacrificing their transparency, owing to its size on the nano-meter scale, reflective index similar to the plastics', excellent mechanical property, and low density. This study investigates effects of CNF on optical, viscoelastic, and thermal properties of CNF reinforced poly(methyl methacrylate) (PMMA). CNF/PMMA with different CNF contents and different types of PMMA were prepared through a solvent casting method with a low toxic and inexpensive solvent, acetone, and compression-molded to create nanocomposite films. The films were characterized using a transmission electron microscope, ultraviolet–visible (UV-Vis) spectrophotometry, dynamic mechanical analysis (DMA), and thermogravimetric analysis (TGA). It was found that CNFs were well-dispersed in the PMMA matrix and the viscoelastic and thermal properties of the PMMA were increased by the addition of CNF, while maintaining a high degree of transparency and increasing attenuation capability of ultraviolet light.

Keywords

Summary for Lay Audience

Cellulose fiber offers an environmentally friendly, sustainable reinforcement option for plastics and can be acquired from a wide range of plant sources along with some animal sources. A cellulose nanofiber (CNF) is a cellulose fiber which has been broken down from a macroscale to a nanoscale. The size reduction creates a fiber with an exceptionally high mechanical properties, providing a unique reinforcement option. Furthermore, CNF exhibits high optical transparency because the fiber diameter is much smaller than the wavelength of visible light. Poly(methyl methacrylate) (PMMA) is a transparent plastic and rivals glass and polycarbonate (PC) for optical transparency. PMMA is lighter than glass and less expensive than PC. However, PMMA possesses relatively low mechanical and thermal properties, which hinders its use in wider applications. In this study, the mechanical and thermal properties of two types of PMMAs were increased by adding CNFs, while maintaining a high degree of their transparency.

Acknowledgments

I am deeply appreciative of the many individuals who have supported me and my work and continually encouraged me throughout this dissertation. Without their time, care, input, encouragement and patience, I would not have been able to see it through.

Special thanks to my supervisor Prof. Takashi Kuboki for his support and dedication to my project and professional development. Thank you for providing me the opportunity to investigate natural fiber polymer nanocomposites. I appreciate the time and effort you provided while we hypothesized and discussed various aspects of this project over the past couple years.

I am grateful to Prof. Sain from the University of Toronto for his advice and support and Prof. Jiang, Prof. Tutunea-Fatan, and Prof. Zhou for being my examiners. I would also like to thank Yixing Tang, Mingyu Yang, and Karen Nygard for their technical support and discussion.

I am grateful for the financial support provided by Ontario Research Fund - Research Excellence (ORF-RE). I also greatly appreciative of Mitsubishi Chemical Corporation and Chuetsu Pulp & Paper Co., Ltd. for supplying materials.

Finally, thank you to my family, friends, and in particular my girlfriend, who have helped me more than they will know. You kept my head straight and allowed me to focus during difficult periods. Your unconditional support in my endeavors is truly appreciated, as I know that without you I would not be writing this.

Table of Contents

List of Tables

List of Figures

Chapter 1

1 Introduction

The term composite refers to a material composed of two or more constituent materials, the combination of which results in novel properties not experienced by either alone. Dating back to ancient Egypt, when straw was added to clay to produce a composite used to build strong buildings, composites have long been a part of human life. Today, a wide variety of materials is available to be used as a matrix and as reinforcement, which enables the ability to create a myriad of composite materials to meet various needs for many applications.

Polymers are poplar materials mainly due to their good processability, low density, and low cost. Polymers also have a wide range of properties, which are governed by the constituents, length, and configuration of molecules to name a few. Unfortunately, polymers are inherently weaker than traditional materials such as ceramics and metals; however, this creates opportunities to add reinforcements, which can enhance the properties of polymers. By selecting a type and amount of a polymer and reinforcement, properties of the resulting composite can be tailored. Common reinforcements in polymer composites are fibers with high modulus and strength such as glass fibers, carbon fibers, and aramid fibers. However, recent environmental concern has led to great interest in utilizing natural fibers to reinforce polymers.

1.1   Research Motivation

Cellulose fiber offers an environmentally friendly, sustainable reinforcement option and can be acquired from a wide range of plant sources along with some animal sources. A cellulose nanofiber (CNF), as the name suggests, is a cellulose fiber which has been broken down from a macroscale to a nanoscale. This removes some of the imperfections in the fiber and increases its aspect ratio (= length/diameter). The size reduction creates a fiber with an exceptionally high Young's modulus and tensile strength, providing a unique reinforcement option. From a functional group perspective, a cellulose nanofiber offers an abundant source of hydroxyl groups and thus plenty of potential chemical interactions with

polymers. Finally, CNF exhibits high optical transparency because the fiber diameter is much smaller than the wavelength of visible light.

Poly(methyl methacrylate) (PMMA) is an amorphous polymer in the acrylate family. Advantages of PMMA stem from its high optical transparency, good scratch resistance, good ultraviolet-light resistance, low density, and low cost. In particular, its excellent optical transparency is an attractive feature. Although PMMA rivals glass and polycarbonate (PC) for optical transparency [1]–[3], PMMA is lighter than glass and offers a shatterproof alternative [4], [5], while being less expensive than PC [4], [5]. However, PMMA possesses relatively low mechanical and thermal properties, which hinders its use in wider applications. Therefore, CNF could be a good candidate to reinforce transparent PMMA.

1.2   Objectives

The main objective of this study is to fabricate cellulose nanofiber reinforced PMMA nanocomposites, and to explore ways of tailoring their physical properties. Specific work included:

(1)   increasing mechanical and thermal properties of PMMA by adding different contents of CNF with a minimum impact on optical properties, and

(2)   increasing mechanical and thermal properties of modified PMMA by adding CNF with minimal impact on optical properties.

1.3   Significance

CNF is easy to agglomerate since it has plenty hydroxyl functional groups. To increase mechanical and thermal properties of PMMA by adding CNF while having a minimal impact on optical properties, it is imperative to uniformly disperse and distribute CNF in the PMMA matrix. In this study, CNF was well dispersed and distributed in the PMMA matrix using a solvent casting method. A low toxic and inexpensive solvent, acetone, was used in this process. The solvent casting method also minimized thermal degradation of CNF during the mixing of CNF and PMMA, unlike melt compounding. This study

demonstrated that the addition of CNF enhanced mechanical properties and thermal stability of PMMA and modified PMMA, while maintaining a high degree of transparency and increasing attenuation capability of ultraviolet light (UV). The CNF/PMMA nanocomposites developed in this study have the combination of good UV resistance and UV attenuation capability, which presents new opportunities for applications where optical transparency and UV transmittance are a field of concern. Furthermore, CNF/modified PMMA nanocomposites developed in this study have the improved properties of the modified PMMA and expand their use for coating applications. Consequently, the research outcome will assist plastic and composite manufacturers in developing CNF/PMMA nanocomposite products.

1.4   Thesis Outline

This thesis is prepared in a monograph format as specified by the School of Graduate and Postdoctoral Studies at Western University, London, Ontario, Canada. This thesis consists of five chapters:

Chapter 1 presents a general introduction, objective, significance, and thesis outline.

Chapter 2 discusses background of PMAA, nanocellulose (including CNF and cellulose nanocrystal (CNC)), manufacturing of nanocellulose/PMMA nanocomposites, and properties of nanocellulose/PMMA nanocomposites.

Chapter 3 presents materials, including PMMA, modified PMMA [copolymers of methyl methacrylate (MMA) and methacrylic acid (MAA)], and CNF, as well as a fabrication method of CNF/PMMA nanocomposites using a solvent casting method. The chapter also introduces characterization methods used in this study (i.e., transmission electron microscopy (TEM), ultraviolet-visible spectrophotometry (UV-Vis), dynamic mechanical analysis (DMA), and thermogravimetric analysis (TGA)).

In Chapter 4, the effects of CNF content as well as MAA content in PMMA on optical, viscoelastic, and thermal properties of CNF/PMMA nanocomposites are investigated.

Chapter 5 summarizes and concludes the thesis and provides some recommendations for future work.

Chapter 2

2   Background

2.1   PMMA

Poly(methyl methacrylate) (PMMA), commercially referred to as acrylic or Plexiglass, is widely used in industry, with its usage expected to grow to 2.85 million tons in 2020, representing USD 10.87 billion [6]. Used in a wide range of fields such as automotive, construction, lighting, biomedical, optical, and sensor applications [4], [5], PMMA provides low density, strong chemical resistance, low moisture absorption, and good insulation [7], while being best known for its optical transparency. PMMA transmits 92% of daylight [2] and possess a refractive index of 1.492 [8]. Although PMMA rivals glass and polycarbonate (PC) for optical transparency [1]–[3], PMMA is lighter than glass and offers a shatterproof alternative [4], [5], while being less expensive than PC [4], [5].

PMMA is also referred to poly [1-(methoxy carbonyl)-1-methyl ethylene] from the hydrocarbon standpoint, and is synthetically produced from polymerization of methyl methacrylate monomers [9]. The structures of both the monomer and the resulting polymer are shown in Figure 1.

Figure 2-1 Polymerization of the methyl methacrylate monomer to poly(methyl methacrylate) [10]

Although detailed discussions about relationships between the structure and properties of PMMA can be found elsewhere [5], some relationships relevant to this study

will be discussed below. PMMA's bulky side groups prevent crystallization and free rotation about the C-C backbone, thus giving PMMA an amorphous structure [5]. Properties of PMMA depend not only on the monomer structure, but also on the secondary and tertiary structures, which designate the configuration of the side chains, otherwise known as tacticity. PMMA can come in the forms of isotactic, syndiotactic, and atactic [5], which are variations in positions of the side chain both along the chain and relative to one another. For example, thermal properties such as the glass transition temperature are based on the tacticty, where syndiotactic, atactic and isotactic PMMA have glass transition temperatures of roughly 130°C, 120°C, and 55°C, respectively [11].

2.2 Nanocellulose

2.2.1 Cellulose

Plants are an exceptional demonstration of nature's ability to develop its own composites to handle the surroundings, and are made of three main constituents: lignin, hemicellulose, and cellulose [12]. The ratio of these constituents varies depending on type of plant and environment, thus resulting in a variety of properties. Lignin is a cross-linked phenolic polymer and functions as the matrix, protecting the cellulose and hemicellulose while providing some strength [13], [14]. Hemicellulose is a copolymer that consists of different monosaccharide and may have a branched structure [13]. Cellulose is part of the fibrous region and offers a high degree of crystallinity and strength and discussed in more details below.

Cellulose, a polysaccharide that is considered to be the most abundant biopolymer on earth [15]–[17], is a linear homopolymer composed of β-1, 4-linked glucose molecules [18], or a linear polymer consisting of two glucose sugar units linked by glucosidic linkages (C-O-C) at the C1 and C4 positions [19], as shown in Figure 2. Each monomer consists of 3 hydroxyl groups, leading to a highly hydrophilic polymer chain.
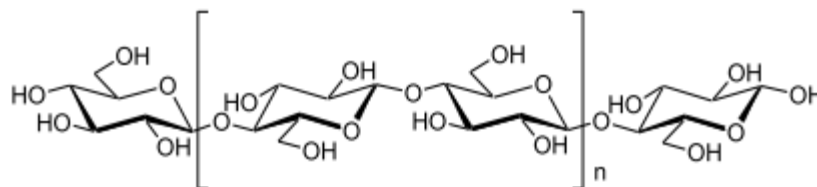
Figure 2-2 Molecular Structure of Cellulose [20] **(Reprinted with permission from ref. 20)**

Cellulose does not commonly exist as a single molecule. During biosynthesis, attraction resulting from Van der Waals and intermolecular hydrogen bonds from the hydroxyls and oxygens of adjacent molecules encourage parallel stacking of multiple cellulose chains, forming groups of elementary fibrils. Aggregating into larger microfibrils or cellulose nanofiber (CNF), the resulting cellulose chains are roughly 5-50nm in diameter and several microns in length [21], [22]. Both crystalline and amorphous regions are formed during biosynthesis [23], as shown in Figure 3.
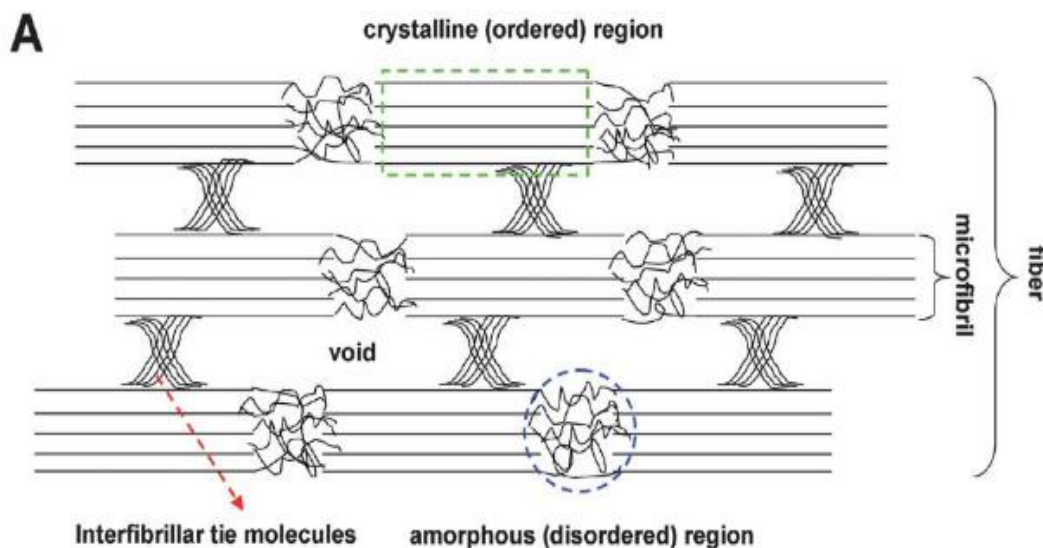
Figure 2-3 Demonstration of cellulose fiber makeup [24] **(reprinted with permission from ref. 24)**

There is a variety of crystalline polymorphs of cellulose; however, cellulose commonly exists in two native states, cellulose I_α and I_β. Both crystal structures can exist within the same source, and each has different properties. Although the relative weighting

varies between sources, it has been reported that similar reinforcing potential is possible [25]. The other polymorphs are not common and usually result from external influences such as mercerization process (i.e., by soaking cellulose in aqueous NaOH), liquid ammonia treatment, and subjugation to high temperatures [26], [27]. The degree of crystallinity in cellulose varies based on the species in question [28]. For example, algal cellulose has an average crystallinity of 68%, while crystallinity of cellulose in natural fibers can range from 41% for mercerized linter cotton to 71% in ramie fibers [29]. Although cellulose has been presented through a discussion of plant fibers, cellulose can be derived from a multitude of sources, including bacteria [30], wood, cotton, sea animals, among others [18], [31]–[35].

In recent years, nanocellulose has gained attention as a reinforcement in polymer nanocomposites, not only because of its low environmental impact, but also because of its excellent physical properties [25], [31], [33], [35], [36], which are driven by the crystalline regions. On the nanoscale, cellulose approaches that of a pure crystal, minimizing surface defects, resulting in exceptional mechanical properties. Unfortunately, isolation of pure crystalline nanocellulose is difficult, and thus properties of the crystalline regions are debated and by no means conclusive. Tashiro et al. [37] theoretically calculated the Young's modulus of crystalline cellulose (I_α) along the chain axis to be 167.5 GPa, more than twice that of aluminum. The modulus of crystalline nanocellulose was reported to be approximately 138 GPa [38], and is generally accepted to be in the range of 100-130 GPa [36]. Nanocellulose also possess low density, which, combined with the high Young's Modulus, makes nanocellulose popular for its specific modulus. For example, with a density of around 1.5-1.6g/cm^3, the specific modulus of nanocellulose is 62.5 kJ/g using a conservative modulus of 100 GPa, whereas traditional glass fibers with a Young's Modulus of 70GPa and density of 2.6 g/cm^3 results in a specific modulus of 27 kJ/g [39]. This demonstrates nanocellulose's remarkable reinforcing potential. Furthermore, nanofibers typically have high aspect ratios, which can also allow for enhancing mechanical properties of polymers.

It should be noted that the functional groups in a cellulose molecule allow for hydrogen bonding between nanocellulose, resulting in both positive and negative effects

with respect to its use as reinforcement. It has been reported that above a certain threshold, nanocellulose can create a percolating network linked by hydrogen bonds, forming a rigid network throughout the composite [40], however; hydrogen bonding can also drive agglomerations [41]. Furthermore, the highly stable hydrogen bonding makes nanocellulose a poor solute, making it difficult to create a uniform dispersion and distribution in hydrophobic polymers. As a result, agglomerations are an often reported issue with nanocellulose and this can affect optical transparency and performance of nanocomposites [42], [43].

2.2.2 Production of Nanocellulose

Advancements in production of nanocellulose over the years have brought down the costs of creating nanocellulose [44]–[46], spurring an increased interest in its use in nanocomposites. Nanocellulose is generally categorized into two main groups: (i) cellulose nanofiber (CNF), also known as cellulose nanofibril, nanofibrillated cellulose, or microfibrillated cellulose and (ii) cellulose nanocrystal (CNC) or cellulose whisker [34]. Commonly, CNF is produced through mechanical shearing processes, which includes both crystalline and amorphous regions, and possess a higher aspect ratio: a diameter of 5–50 nm and a length of a few micrometers. In contrast, CNC are typically produced through acid hydrolysis of cellulose, which dissolves the amorphous regions while leaving the crystalline regions and has a diameter of 3–35 nm and a length of 200–500 nm.

2.2.2.1   Mechanical Processing

Mechanical processing involves subjecting cellulose fibers to high shear or normal stresses to separate the bundles into smaller fibers. The resulting fibers are commonly referred to as cellulose nanofiber (CNF), and have been obtained from a wide variety of sources, including wood [47], tunicate [48], banana [49], pineapple leaf [50], bamboo [51], cotton [52], algae [53], sludge [44], other industrial residues [46], etc. The dimensions of the resulting fibers are dependent on the source [21].

There are different procedures to produce CNF under the mechanical processing umbrella, including high-pressure homogenization [54]–[57] and/or grinding [58],

grinders/refiners [47], [59] cryocrushing, [56], [60] and high intensity ultrasonic treatments [61]–[63].

High pressure homogenization applies high shear forces to cellulose fibers, breaking them apart and promoting fibrillation [36], which results in a web-like structure [64]. This must be iterated through multiple cycles, creating a more homogeneous distribution of fiber geometric with increasing cycles, and have created fibers with 10-100nm diameter [65]. This iterative method makes the process more energy intensive. Nakagaito et al. [66] found that there were minimal improvements in mechanical properties of the polymer by addition of the CNF below 30 passes, whereas there was a step increase in the Young's Modulus of 50% above 30 passes. Zimmerman et al. [54] also found that the inhomogeneities of fibers decreased mechanical properties of the composites dramatically, demonstrating that quality of fibrillation is crucial for the resulting composite properties.

Ultrasonciation involves subjecting cellulose fibers to high frequency vibrations, producing an oscillatory behavior [62], breaking larger fiber bundles into smaller ones, which disaggregates and increases their surface area [23], [67]. This allows for the retention of their fibrous texture, considering the cellulose fibers are vibrated apart rather than being mechanical sheared and broken [68], which maintains the geometries and results in high aspect ratio fibers [23]. The effectiveness is dependent on the power, concentration, temperature, size and time [62].

2.2.2.2 Chemical Processing

Chemical processing involves subjecting cellulose fibers to a strong acid, which begins to attack the cellulose. The amorphous region, being more susceptible, degrades and the long chain breaks apart into shorter, highly crystalline chains [69], [70]. These fibers are commonly designated cellulose nanocrystal (CNC). Similar to the mechanical processing, chemical processing has been applied to a wide variety of sources, such as softwood pulp [71], cotton [70], sisal [72], microcrystalline cellulose [73], bacterial cellulose [74], soy hulls [75], whose choice also impacts the final product [76]. Similar to CNF, CNC has an exceptionally large surface area with plenty of hydroxyl groups; however, the aspect ratio

is reduced. The highly crystalline nature results in fibers with a reported tensile strength of 7500 MPa and Young's Modulus of 100-140 GPa [77].

There is a wide variety of acids to choose from for this processing. For example, sulfuric [78]–[80], hydrochloric [23], [81], hydrobromic [82], and nitric acids [83] have been used to produce CNC. Under sulfuric acid hydrolysis, the hydroxyl groups undergo esterification, yielding half-esters, resulting in a product referred to as cellulose sulfate. The surface sulfate groups leave a negative charge, electrostatically repelling adjacent fibers and preventing agglomeration [84], [85] while facilitating a homogeneous dispersion [24]. The thermal stability is also affected by the resulting negative charge, where Roman et al. [86] noted that both degradation temperature and activation energy decreased with increasing sulfate groups in bacterial cellulose, and recommended that to maintain thermostability, esterification should be kept to a minimum. Furthermore, sulfuric acid was noted to significantly reduce the cellulose I structure, making cellulose II more prevalent [87].

It was reported that CNC produced through sulfuric acid had a yellowing appearance [70] which began at 60°C and intensified up to 160°C where they turned nut brown [88]. Comparatively, CNC's produced through other acids like hydrochloric acid were thermally stable up to 220°C [88], though agglomerations still occurred since hydrochloric acid did not affect surface charge of cellulose [89]. CNC produced through phosphoric acid began to yellow at 160°C but did not begin to degrade until 220°C [88].

The acid chosen also has effects on the resulting solvent suspension. Espinosa et al. [88] investigated the dispersion of sulfuric acid CNC (S-CNC), hydrochloric acid CNC (H-CNC), and phosphoric acid CNC (P-CNC) in solvents with different polarities – H_2O, dimethyl sulfoxide (DMSO), dimethylformamide (DMF), and tetrahydrofuran (THF). All samples were kept to a concentration of 9 mg/ml and were ultrasonicated to create the initial dispersion. None of the CNC types dispersed well in THF, while all other solvents maintained stable dispersions for 1 day after ultrasonication. P-CNC's were found to create stable dispersions up to 2 months, whereas the S-CNC's started to phase-separate after 10 days in DMSO. H-CNC's started to phase-separate from all solvents after 10 days. Through

TEM observations, P-CNC and S-CNC were well dispersed in H_2O, DMSO, and DMF, while H-CNC's showed aggregates, except for the dispersion in DMF. Dispersibility of P-CNCs in DMSO was better than that of S-CNC, which were attributed to the extra OH group present on the phosphate.

The study then followed up by creating CNC reinforced polyamide 12 (PA12) through (i) solvent casting from DMF (dried at 70C and then compression molded at 190C) and (ii) melt-compounding [90]. CNC was produced from cotton (c) and tunicate (t). The P-cCNC based composites did not show yellowing, but the S-cCNC and S-tCNC based composites were very yellow. The S-CNC based composites had thermal stability of 180°C while the P-CNC based composites was 290°C. When composite fabrication methods were compared (i.e., the solvent casting vs. melt-compounding), under solution casting, P-cCNC and S-cCNC based composites produced through the solvent casting showed similar increases in storage modulus, while under the melt-compounding, P-cCNC based composites had higher storage modulus than S-cCNC based composites.

2.3   Manufacturing of Nanocellulose/Polymer Nanocomposites

Appropriate manufacturing processes are necessary in order to create nanocellulose/polymer composites with desired properties, size, and shape. Creating a uniform dispersion and distribution of nanocellulose in polymers has received a lot of attention, leading to many different processing techniques including melt processing and solvent casting [91], [92]. Solvent casting is a favorable process to produce nanocomposites with polymers that would be incompatible with nanocellulose. By suspending nanocellulose in a solvent, a good dispersion and distribution of nanocellulose can be achieved by cellulose-solvent interactions rather than cellulose-cellulose interactions. Nanocomposites can be produced by introducing polymer and nanocellulose to the solvent and evaporating the solvent. The nanocomposites are then shaped with appropriate size for testing using compression molding. The solvent casting and compression molding are discussed in more details below.

2.3.1   Solvent Casting

Solvent casting is a simple method to manufacture polymer composites [20]. Particularly on a small scale, solvent casting is favored for its ease of fabrication without requiring any specialized equipment or damaging fibers.

Solvent casting involves dispersing both polymer and fibers in a solvent, which acts as the medium, demonstrated in Figure 4. The solvent must penetrate and disentangle the polymer chains, which causes swelling of the polymer. This disentanglement can occur only if the polymer/solvent interaction is thermodynamically favored. After the polymer is dissolved in the solvent, fibers are added and mixed, creating a homogeneous polymer/fiber/solvent solution. The solvent is then evaporated, ideally resulting in a uniform distribution of the fibers in the polymer matrix.
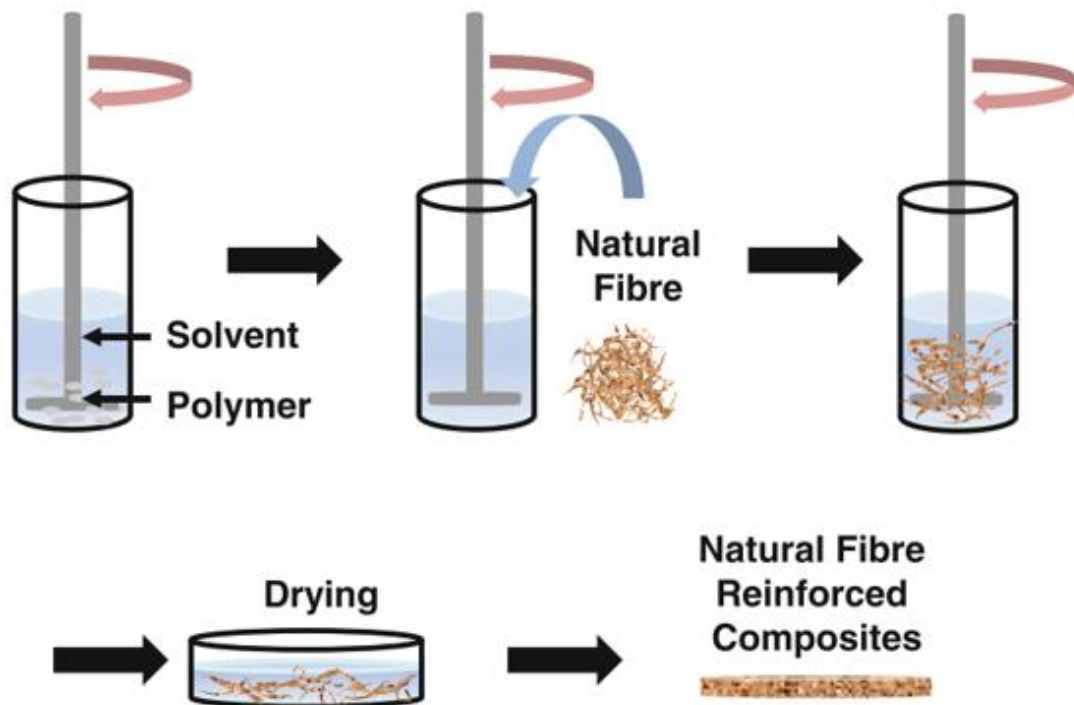
Figure 2-4 Demonstration of Solvent Casting Process [93]

Solvent casting is beneficial in that it improves mixing of polymers and fibers. Compared to melt mixing, mixing of fibers in polymer solutions greatly improve a degree of fiber dispersion [93].

Many variables affect solvent casting effectiveness, including types of polymers (composition, stereochemistry, molecular weight, tacticity, and conformation) and processing conditions [93]. Moreover, choice of solvent largely influences the effectiveness of solvent casting. Configuration of polymer chains in a solution is governed by types of solvents. If the polymer-solvent interactions are greater than polymer-polymer interactions, chain segment will extend by diffusion of solvent molecules, thus extending the polymer chains and increasing the free volume of the polymers. Conversely, if the polymer-solvent interactions are smaller than polymer-polymer interactions, the polymer chains contract, thus hindering dispersion of polymer chains in the solvent and thus the ability to form polymer-fiber interactions, demonstrated in Figure 5.

Poor Solvent   Good Solvent
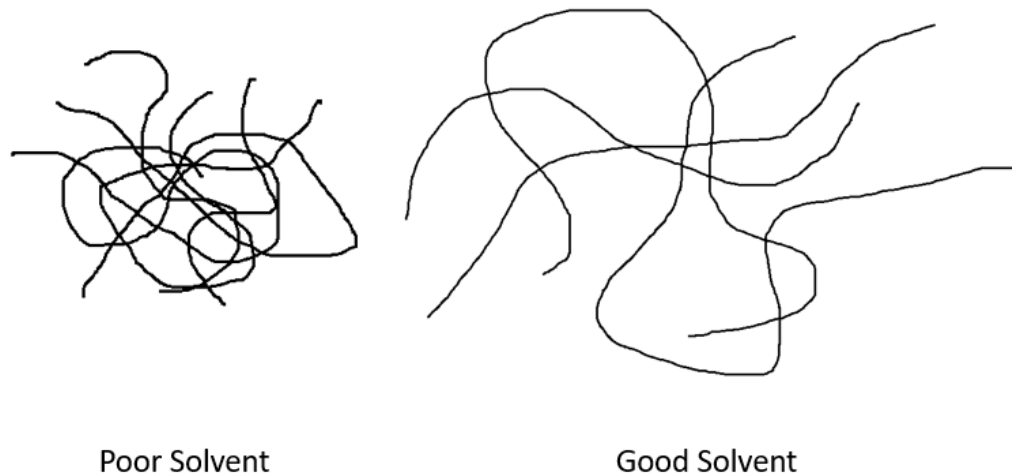
Figure 2-5 Effect of Solvent on Random Coil Radius of Polymer Chains

Unfortunately, there are negative effects of solvent casting on performance of the resulting composites. When the solvent is evaporated from polymer/fiber/solvent solution, some solvent may remain bonded to the polymer or fiber because the solvent may have a strong interaction with the polymer chains and/or fibers, decrease physical properties of the composites. Furthermore, residual solvent may exist at the interface between the polymer matrix and fibers, which decreases the polymer/fiber interfacial bonding and negatively affects the mechanical properties [94]. Therefore, it is important to remove the solvent completely; however, is not an easy task to remove a solvent which has a high

boiling point or is well bonded. Another issue is that solvent casting requires a relatively large amount of solvent, which is not a cost-effective process in industrial setting. In addition, solvent casting is a batch process and prevents mass production.

When nanocellulose is used as fiber, due to its polar nature, the solvent used may be required to be polar and possess a high dielectric constant and dipole moment to achieve a stable dispersion of nanocellulose in the solvent [95] A nonpolar solvent likely leads to agglomerations of nanocellulose that have negative impacts on the mechanical properties and transparency of the composites [43], [96], [97].

Another consideration of solvent selection is health risk. For example, acetone is one of the three ketone bodies that occur naturally within the body. As a solvent, it is relatively less toxic than many other industrial solvents and can be considered a weak irritant. Conversely, Dimethylformamide (DMF) has been shown to be hepatotoxic in animal and humans in both acute and repeated dose studies [98], [99].

2.3.2 Compression Molding

Compression molding is often used to shape composite materials with proper size. In the compression molding process, a specified amount or 'charge' of the composite material is placed in a mold which is situated between two plates. The charge is then compressed between the plates, forcing the charge to conform to the geometry of the mold cavity. This process can be performed through either a hot or cold press. Under hot compression, the plates are heated, which allows the charge to warm up and flow easily into the mold cavity during compression. Cold compression involves simply applying pressure to the charge at room temperature [93].

The main advantage with compression molding is that, if a mold cavity is small, the resulting composites largely conserve isotropic properties. Furthermore, compression molding prevents reductions in fiber length during processing, unlike injection molding [93]. These advantages allow compression molding to produce a composite product with good properties. Other advantages stem from the reproducibility and low cycle time [93]. As a result, compression molding is an appropriate method in the production of composites.

The main area of concern in this process is, if a mold cavity is large, flow of the charge into the mold. Movement over long distances in the mold cavity will tend to cause separation of the polymer matrix and fibers and anisotropic fiber orientation. Another issue is that air must be pushed out from the mold. Otherwise, voids will be generated in the resulting composites, which negatively affects their properties.

2.4 Properties of Nanocellulose/PMMA Nanocomposites

Important properties of nanocellulose/PMMA nanocomposites are optical, viscoelastic, and thermal properties. Literature related to these properties is reviewed as follows.

2.4.1 Optical Properties

Transparency, being one of PMMA's primary benefits, needs to be retained in nanocellulose/PMMA nanocomposites. This is best achieved by homogeneously dispersing and distributing nanocellulose in PMMA and minimizing agglomerations or large clumps of nanocellulose [43], [97], [100]. Table 1 summarizes the effects of the addition of nanocellulose on transparency of nanocellulose/PMMA nanocomposites reported in the past, where various types (including surface modification) and amount of nanocellulose were investigated. The transparency data are presented at different wavelengths (from 400 to 700 nm), and all possible data has been normalized to 0.3 mm thickness through the Beer-Lambert law. It is noted that thickness data were not provided in the study by Kiziltas et al. [97].

Table 2-1 Transmittance of Nanocellulose/PMMA Nanocomposites.

Type of Nanocellulose	Nanocellulose Content (Wt %)	Transparency (%)				Reference
		400 nm	550 nm	600 nm	700 nm	
CNC	0.1	80.6	85.4	87.1	89.1	Anzlovar et al. [43]
CPADB-CNC[2]	0.1	75.9	77.0	76.4	77.9	Anzlovar et al. [43]
PMMA-CNC[3]	0.1	65.3	75.7	75.7	75.7	Anzlovar et al. [43]
CNF	0.25	22		21		Kiziltas et al. [97][1]
CNC	0.25	74		72		Kiziltas et al. [97][1]
CNF	0.5	8		4.5		Kiziltas et al. [97][1]
CNC	0.5	56		55		Kiziltas et al. [97][1]
CNF	1	57.7	69.9	72.1	77.9	Littunen et al. [101]
PMMA-CNF[4]	1	53.3	61.1	64.4	68.3	Littunen et al. [101]
CNF	5	48.6	62.8	70.6	77.2	Littunen et al. [101]
PMMA-CNF[4]	5	60.3	75.1	77.2	80.7	Littunen et al. [101]
PEG-NH$_2$-TEMPO-CNF	5	61.4	70.5	70.5	72.9	Huang et al. [102]
CNC	5	54.3	63.8	65.3	69.7	Liu et al. [42]
In situ MA-CNF[5]	10	88.4	89.1	89.8	89.5	Sain et al. [100]
Ex situ MA-CNF[5]	10	75.9	77.0	76.4	77.9	Sain et al. [100]
CNC	10	37.3	45.6	48	53.3	Liu et al. [42]
TEMPO-CNF	12.9	65.3	75.7	75.7	75.7	Fujisawa et al. [103]
CNF	30	0.7	2.2	2.7	3.2	Boujemaoui et al. [104]
mCNF-b-PMMA[6]	38	1.6	7.4	9.1	12.5	Boujemaoui et al. [104]
mCNF-g-PMMA[7]	38	8.5	15.8	18.5	21.6	Boujemaoui et al. [104]

[1] No film thickness data was provided to normalize the data.
[2] CNC was grafted with a reversible addition-fragmentation chain transfer (RAFT) agent, 4-cyano-4-(phenylcarbonothioylthio)pentanoic acid (CPADB).
[3] PMMA was grafted onto CPADB-CNC.
[4] PMMA was covalently grafted onto CNF.
[5] CNF was chemically modified with maleic anhydride.
[6] CNF was modified with Allyl Glycidyl Ether (AGE) and mixed with PMMA.
[7] PMMA was grafted onto mCNF and then blended with PMMA.

The table showed a trend that transparency is lower at lower wavelengths. Aside from CNF data from Kiziltas et al., transparency also decreases with increasing nanocellulose content. There is little data regarding CNC data; however, it appears that CNC provides a higher transparency than CNF, though this conclusion is mainly drawn from Kiziltas' data [97]. Compatibility between nanocellulose and PMMA can play a role in transmittance. Anzlovar et al. [43] observed that transmittance decreased in the order of PMMA-NCC, CPADB-NCC, and NCC, which theoretically correlated to the order of their compatibility with PMMA. This idea was echoed by Boujemaoui et al. [104], who reported that diffraction may occur at an interface, especially in the presence of nanoscale air voids. The higher transmittance of mCNF-g-PMMA was a result of the better fiber distribution and covalent bonding at the interface between CNF and PMMA [104]. Sain et al. [100]

reported that maleic anhydride modified CNF, both through the *in situ* and *ex situ* process, provided exceptionally high transparency. Fujisawa et al [103] also reported exceptionally high transparency using TEMPO modified CNF. However, in the study by Littunen et al. [101], transmittance was reduced as a result of the increased compatibility between modified CNF and PMMA. They claimed that the reduction of transmittance resulted from inability of the immobilized polymer on the fiber to completely blend with the bulk polymer, thus increasing the size of opaque domains [101].

2.4.2 Viscoelastic Properties

Table 2 summarizes the effects of the addition of nanocellulose on storage modulus of nanocellulose/PMMA nanocomposites reported in the past, where various types (including surface modification) and amount of nanocellulose were investigated. The percentage increase of storage modulus of nanocomposites from the neat PMMA's is presented. Through a cursory analysis, addition of neat nanocellulose increased storage modulus with increasing nanocellulose content, though it is small. Through surface modifications, a larger increase in storage modulus was obtained.

Table 2-2 Storage Modulus of Nanocellulose/PMMA Nanocomposites.

Type of Nanocellulose	Nanocellulose Content (Wt %)	Testing Temperature	Storage Modulus (% increase)	Reference
CNC	0.25	Room temperature	2.6	Kiziltas et. al [97]
CNF	0.25	Room temperature	1.5	Kiziltas et. al [97]
CNC	0.5	Room temperature	5.5	Kiziltas et. al [97]
CNF	0.5	Room temperature	8.8	Kiziltas et. al [97]
CNF[3]	2.5	40°C	4.85	Anju et. al [105]
Si69-CNF[1]	2.5	40°C	19.4	Anju et. al [105]
CNF[3]	5	40°C	11.57	Anju et. al [105]
Si69-CNF[1]	5	40°C	19.4	Anju et. al [105]
CNF[3]	10	40°C	23.13	Anju et. al [105]
Si69-CNF[1]	10	40°C	35.82	Anju et. al [105]
TEMPO-CNF[2]	12.9	50°C	82.61	Fujisawa et. al [103]
CNF[3]	15	40°C	17.91	Anju et. al [105]
Si69-CNF[1]	15	40°C	51.49	Anju et. al [105]

[1]Bis-(3-triethoxysilylpropyl)tetrasulphide was added to CNF/PMMA mixture to improve interfacial interactions
[2]HCl was used to enhance dispersion of TEMPO-NFC

Kiziltas et al. attributed the increase in storage modulus, particularly at higher temperatures, to nanocellulose's ability to restrict motions of PMMA chains [97]. On the other hand, Anju et al. reported that addition of more than 10 wt% CNF decreased storage modulus (optimum loading was at 10wt%) and attributed the decrease to agglomerations of CNF, while samples with compatibilizer (Si69) showed continual increase of storage modulus with increasing CNF content [105]. Fujisawa plotted their data against the percolation model, which fit their data well, and used it to conclude that the network formation that occurred had a large contribution on the increase of storage modulus, particularly at higher temperatures, along with well-dispersed CNF in the matrix [103].

Table 3 summarizes the effects of the addition of nanocellulose on tan δ peak value of nanocellulose/PMMA nanocomposites reported in the past, where various types (including surface modification) and amount of nanocellulose were investigated. Tan δ is defined as a ratio of loss modulus to storage modulus. Kiziltas et al. [97] showed that tan δ peak decreased with increasing nanocellulose content and attributed the decrease to restriction of chain segment mobility. Similar phenomenon was reported in other

nanocomposites [65], [75], [94], [106]–[111]. Contrarily, Anju [105] showed that addition of CNF increased tan δ peak value, which means that the resulting nanocomposite was more viscous and less elastic.

Table 2-3 Tan δ Peak Value of Nanocellulose/PMMA Nanocomposites.

Type of Nanocellulose	Nanocellulose Content (Wt %)	Temperature (ºC)	Tan Delta Peak	Reference
PMMA			0.99	Kiziltas et al. [97]
CNF	0.25		0.96	
CNC	0.25		0.81	
CNF	0.5		0.86	
CNC	0.5		0.65	
PMMA	0	93.8	1.25	Anju et al. [105]
CNF	2.5	92.16	1.1	
Si69-CNF	2.5	96.83	1.29	
CNF	5	93.6	1.2	
Si69-CNF	5	99.3	1.42	
CNF	7.5	95.67	1.25	
Si69-CNF	7.5	101.1	1.37	
CNF	10	97.5	1.3	
Si69-CNF	10	104.5	1.42	
CNF	12.5	98.6	1.36	
Si69-CNF	12.5	101.9	1.31	
CNF	15	99.6	1.42	
Si69-CNF	15	105.67	1.18	

2.4.3 Thermal Properties

Table 4 summarizes the effects of the addition of nanocellulose on glass transition temperature (Tg) of nanocellulose/PMMA nanocomposites reported in the past, where various types (including surface modification) and amount of nanocellulose were investigated. The increase or decrease in Tg (ºC) of nanocomposites from the neat PMMA's is presented. Overall, the data do not present a clear trend regarding the effect of nanocellulose content on Tg. Whenever there was an increase in Tg, it was explained by decreased mobility of polymer segments [97], [100], [103], [104], [112], whereas a decrease in Tg was explained by enhanced mobility of polymer segments [42], [87], [101].

Table 2-4 Glass Transition Temperature of Nanocellulose/PMMA Nanocomposites.

Type of Nanocellulose	Nanocellulose Content (Wt %)	Glass Transition Temperature (°C increase/decrease)	Reference
NFC	0.25	3.64	Kiziltas et al. [97]
NFC	0.25	0.38	Kiziltas et al. [97]
PMMA/CNP[1]	0.3	-8	Sain et al. [87]
CNC	0.5	6.8	Kiziltas et al. [97]
CNC	0.5	4.54	Kiziltas et al. [97]
CNF	0.5	-10	Littunen et al. [101]
PMMA-CNF[3]	0.5	-11	Littunen et al. [101]
CNF	1	-20	Littunen et al. [101]
PMMA-CNF[3]	1	-7	Littunen et al. [101]
TEMPO-CNF[4]	1.3	3	Fujisawa et al. [103]
CNC	2	-2.8	Liu et al. [42]
CNF	2.5	-2	Anju et al. [105]
Si69-CNF[5]	2.5	6	Anju et al. [105]
CNC	3	-20.1	Liu et al. [42]
CNF	5	-6	Littunen et al. [101]
PMMA-CNF[3]	5	-8	Littunen et al. [101]
CNF	5	0	Anju et al. [105]
Si69-MCC[5]	5	7	Anju et al. [105]
CNC	5	-19.1	Liu et al. [42]
CNF	7.5	4	Anju et al. [105]
Si69-CNF[5]	7.5	11	Anju et al. [105]
CNC	8	-21.5	Liu et al. [42]
MMIPC[2]	10	19	Banerjee et al. [112]
MMEPC[2]	10	12	Banerjee et al. [112]
IPMC[6]	10	22	Sain et al. [100]
EPMC[7]	10	15	Sain et al. [100]
CNF	10	6	Anju et al. [105]
Si69-CNF[5]	10	12	Anju et al. [105]
CNC	10	-19.8	Liu et al. [42]
CNF	12.5	7	Anju et al. [105]
Si69-CNF[5]	12.5	14	Anju et al. [105]
TEMPO-CNF[4]	12.9	3.8	Fujisawa et al. [103]
CNF	15	-12	Littunen et al. [101]
PMMA-CNF[3]	15	-20	Littunen et al. [101]
CNF	15	8	Anju et al. [105]
Si69-CNF[5]	15	14	Anju et al. [105]
CNF-b-PMMA	30	-1	Boujemaoui et al. [104]
TEMPO-NFC	30.77	8.4	Fujisawa et al. [103]
mCNF-b-PMMA[8]	38	20	Boujemaoui et al. [104]
mCNF-g-PMMA[9]	38	5	Boujemaoui et al. [104]

[1] Reported as a cellulose nanoparticle, which is likely equal to CNC

[2] MMA grafted onto nanocelluose

[3] PMMA was covalently grafted onto CNF

[4] NFC was oxidized with TEMPO

[5] Bis-(3-triethoxysilylpropyl)tetrasulphide was added to CNF/PMMA mixture to improve interfacial interactions

[6] Maleic anhydride modified CNF prepared through an *in situ* process

[7] Maleic anhydride modified CNF prepared through an *ex situ* process
[8] CNF was modified with allyl glycidyl ether (AGE) and mixed with PMMA.
[9] PMMA was grafted onto mCNF and then blended with PMMA.

Some explanations were made about the increase of Tg as a result of the addition of nanocellulose. It was suggested that the increase of Tg was caused by interaction between hydroxyl groups in nanocellulose and carbonyl groups in PMMA [97], [112]. For modified CNF [104], Boujemaoui et al. suggested hydrogen bonding between MMA-modified CNF and ester groups of PMMA molecules increased Tg. For other modified CNF [104], they suggested that better distribution of mCNF, which was concluded from optical properties, caused a larger amount of PMMA to be affected by CNF and increased Tg. Interestingly, mCNF-g-PMMA had a lower Tg than mCNF-b-PMMA, though it should have stronger interactions theoretically. This could have been a result of minor differences in polymer structure formed during the grafting approach or physical aging effects [104]. Anju et al. [105] suggested that increase of Tg is due to restriction of segmental mobility of PMMA from the good dispersion of CNF.

Table 5 summarizes the effects of the addition of nanocellulose on thermal decomposition temperature of nanocellulose/PMMA nanocomposites reported in the past, where various types (including surface modification) and amount of nanocellulose were investigated. Thermal decomposition temperatures at 10% and 50% mass loss are presented. Similar to the Tg results, the data do not present a clear trend regarding the effect of nanocellulose content on thermal decomposition temperature at 10% mass loss, whereas thermal decomposition temperature at 50 % mass loss tends to increase with increasing nanocellulose content, though some data showed decreases.

Table 2-5 Thermal Decomposition Temperature of Nanocellulose/PMMA

Nanocomposites

Type of Nanocellulose	Nanocellulose Content (Wt %)	Decomposition Temperature at 10% Mass Loss	Decomposition Temperature at 50% Mass Loss	Reference
PMMA	0		346	Sain et al. [87]
CNC[1]	0.3		320	
PMMA	0	305	368	Kiziltas et al. [97]
CNF	0.25	325	370	
CNC	0.25	321	370	
CNF	0.5	319	371	
CNC	0.5	292	373	
PMMA	0	177	330	Banerjee et al. [112]
MMIPC[2]	10	290	350	
MMEPC[3]	10	160	350	
PMMA	0	100	286	Sain et al. [100]
IPMC[4]	10	270	340	
EPMC[5]	10	140	355	
PMMA	0	345	377	Huang et al. [102]
TOCN[6]	1	340	376	
TOCN[6]	3	350	381	
TOCN[6]	5	340	384	
TOCN[6]	10	275	373	
PMMA	0	263	350	Boujemaoui et al. [104]
CNF-b-PMMA	30	291	385	
mCNF-b-PMMA[7]	38	277	380	
mCNF-g-PMMA[8]	38	303.5	400	

[1]Cellulose Nanoparticle (most likely CNC equivalent)
[2]MMA grafted onto CNF prepared through an *in situ* process
[3]MMA grafted onto CNF prepared through an *ex situ* process
[4]Maleic anhydride modified CNF prepared through an *in situ* process
[5]Maleic anhydride modified CNF prepared through an *ex situ* process
[6]TEMPO oxidized CNF
[7] CNF was modified with allyl glycidyl ether (AGE) and mixed with PMMA.
[8] PMMA was grafted onto mCNF and then blended with PMMA.

Some explanations were made regarding the effects of nanocellulose on thermal decomposition temperature of nanocellulose/PMMA nanocomposites. Sain et al. [87] observed that the addition of CNC decreased thermal decomposition temperature and suggested that the CNC affected entanglement of the polymer chains. In contrast, other researchers [97], [104] observed that addition of CNF increased thermal decomposition

temperature and attributed the increases to hydrogen bonding between CNF and PMMA, as it was reported that hydrogen bonding had a positive effect on thermal stability of other composites [7]. Addition of modified CNF also increased thermal stability of PMMA due to enhanced bonding between CNF and PMMA [100], [112]. Furthermore, it was reported that sample preparation possibly had an impact on heat transfer within the samples during TGA experiments [97], [100], based on the resulting size, morphology, and homogeneity.

Chapter 3

3   Experimental

3.1   Materials and Fabrication of Nanocomposites

Three types of PMMA with a weight-average molecular weight of 90 kg/mol was supplied in the form of powder by Mitsubishi Chemical Corporation. One is a homopolymer of methyl methacrylate (MMA) and the other two are copolymers of methyl methacrylate (MMA) and methacrylic acid (MAA). Chemical structures of MMA and MAA and their compositions are shown in Figure 6 and Table 7, respectively. Addition of MAA could improve adhesiveness of PMMA to other materials, which is suitable for coating applications. CNF in a water suspension (nanoforest-S) was supplied by Chuetsu Pulp & Paper Co., Ltd. Acetone (Purity > 99.9%) was purchased from Caledon Laboratories Ltd.

(a)   (b)
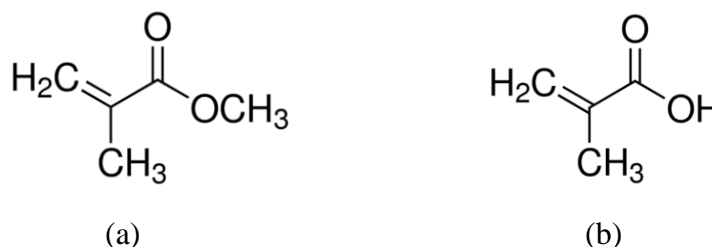
Figure 3-1 Chemical structures of (a) methyl methacrylate (MMA) and (b) methacrylic acid (MAA)

Table 3-1 Monomer compositions of PMMA-based materials used in this study.

Name	MMA (wt%)	MAA (wt%)
PMMA	100	
PMMA0.5	99.5	0.5
PMMA2.0	98	2

First, PMMA powder (either PMMA, PMMA0.5, or PMMA2.0) was dried in an oven at 80°C for 3 hours to remove moisture. The powder was then dissolved in acetone through mechanical stirring with a magnetic stirrer. CNF/acetone mixture was prepared from CNF/water mixture through a solvent exchange method using a centrifuging process. The PMMA/acetone solution was mixed with the CNF/acetone mixture to create different weight percentages of CNF with respect to PMMA, as summarized in Table 7. The suspension of CNF/PMMA/acetone was then sonicated and mechanically stirred with a magnetic stirrer to disaggregate agglomerations and to create a homogenous distribution of CNF. Finally, the suspension was poured into a petri dish and dried.

The resulting films were cut into small pieces and oven dried above acetone's boiling point for 3 days, followed by hot-pressing at 180°C to create CNF/PMMA film samples. The thickness of samples was 300 μm.

Table 3-2 Formulations of CNF/PMMA nanocomposites prepared in this study.

	PMMA (wt%)	PMMA0.5 (wt%)	PMMA2.0 (wt%)	CNF (wt%)
1	100.0			0
2	99.0			1.0
3	98.0			2.0
4	97.1			2.9
5	95.2			4.8
6		100.0		0
7		95.2		4.8
8			100.0	0
9			95.2	4.8

3.2   Transmission Electron Microscopy

Transmission electron microscopy (TEM) is a characterization method in which a beam of electrons is transmitted through a specimen to form an image. TEM is capable of imaging

at a significantly higher resolution than transmission light microscopy (LM). A depiction of TEM is shown in Figure 7. In LM, at first light is refracted through a condenser lens. The light beam then passes through a specimen and is projected onto the eye through objective and projective lenses. In TEM, an illumination source is an electron emitter. Lenses are used to refract electrons onto a specimen and eventually on the fluorescent screen.
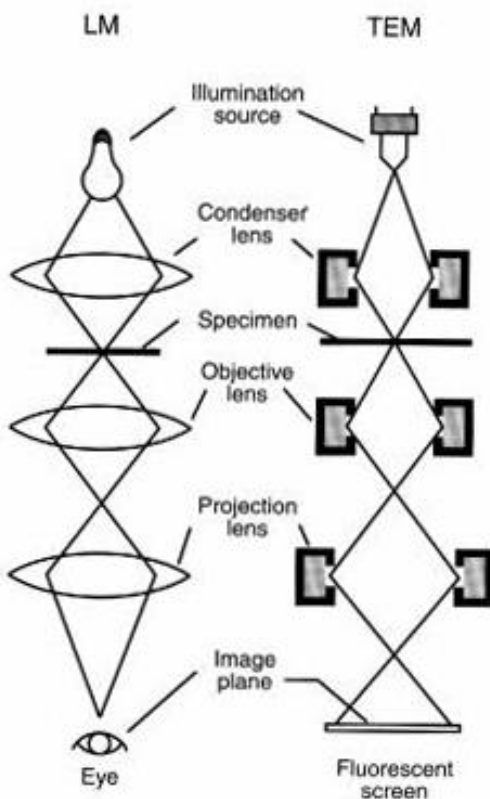
Figure 3-2 Similarities between TEM and LM [113]

TEM is a useful characterization technique to investigate dispersion and distribution of CNF in PMMA. Agglomerated CNF decreases transparency and mechanical properties of the nanocomposites. In addition, TEM enables the ability to observe the orientation of CNF in PMMA, which affects isotropy of the nanocomposites.

In this study, morphology of the nanocomposites was observed using a transmission electron microscope (CM10, Philips Electronics) operated at 60 kV. Thin samples of

approximately 100 nm in thickness were prepared using an ultra-microtome (Ultracut E, Reichert-Jung) with a Diatome diamond knife, and then stained with 2% w/v aqueous solution of uranyl acetate for 5 minutes.

3.3   Ultraviolet-Visible Spectrophotometry

Ultraviolet-visible spectrophotometry (UV-Vis) is a characterization technique to measure absorbance or transmittance of light passing through a sample in the ultraviolet and visible spectral regions. Schematic of UV-Vis is shown in Figure 8. The 'white light' emitted from a light source passes through a diffraction grating unit, which, as a prism, separates the white light into its constituent wavelengths and refracts them at different angles. Only light with a particular wavelength can pass through an adjustable narrow slit. The light is then split into two beams before it reaches a sample. One beam passes through the sample while the other beam does through a reference cell. Eventually, both lights pass through a detector. The detector measures the amount of absorbance from the sample compared to that of the reference cell.
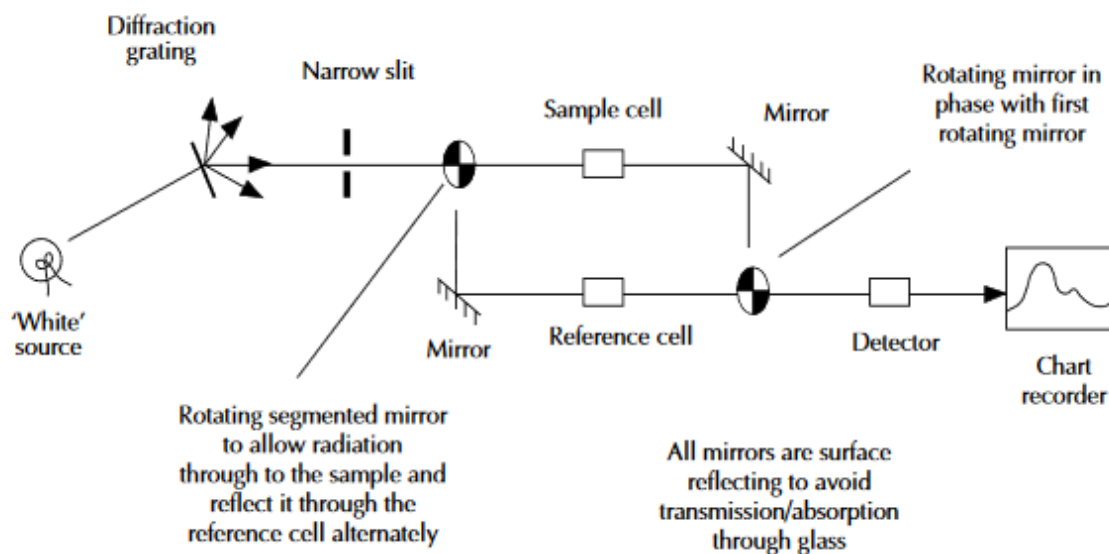
Figure 3-3 Working principle of UV-Vis [114]

The absorbance can be expressed using the Beer-Lambert law [115]:

$$A = \varepsilon c L \qquad\qquad (3.1)$$

where A is the absorbance, ε is a constant known as the molar absorptivity, c is the concentration of the absorbing species, and L is the path length through the sample (or sample thickness in this study). Since the absorbance is proportional to the sample thickness, the absorbance of samples with difference thicknesses can be normalized with thickness.

The transmittance of a material can be related to the absorbance of the material through the following relationship:

$$T(\%) = 10^{(2-A)} \tag{3.2}$$

where T (%) is the transmittance in percentage and A is the absorbance at a given wavelength.

Two transmission measurements are possible: direct transmittance and total transmittance. The direct transmittance is a measurement of the amount of initial light that lands incident on the detector, and thus does not account for any light that may have been refracted. This method is commonly applied in transparent materials. On the other hand, the total transmittance is a measure of the total amount of initial light that makes it through the sample, including that which is refracted at an angle. This is commonly applied in hazy materials, where much of the initial light is refracted, rather than passing directly through the sample.

In this study, direct transmission spectra of the nanocomposites were measured using an ultraviolet–visible-near Infrared (UV-Vis-NIR) spectrophotometer (UV-3600, Shimadzu). Air was used as reference.

3.4   Dynamic Mechanical Analysis

Dynamic Mechanical Analysis (DMA) is a versatile characterization method that measures viscoelastic properties of a specimen. A specimen is subjected to deformation under a temperature or frequency sweep as shown in Figure 9.
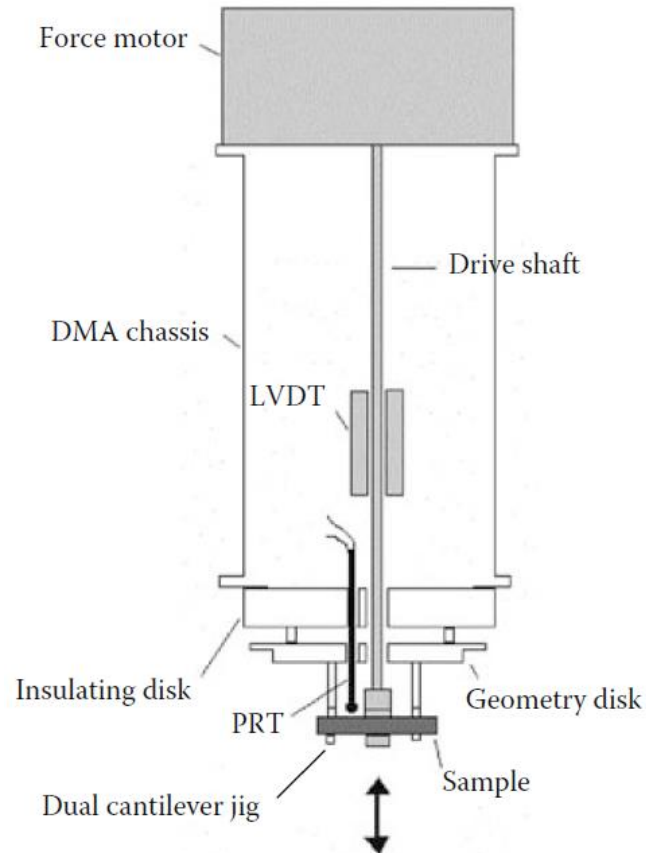
Figure 3-4 Schematic of DMA [116]

The DMA applies an oscillatory force (or stress) to a sample, which generates an oscillatory deformation (or strain), as shown in Figure 10. Under the applied sinusoidal wave, the in-phase component represents the elastic component, while the out of phase component represents the viscous component. By measuring the force and deformation as well as the lag between the force and deformation sine waves, properties such as elastic component of modulus (storage modulus), viscous component of modulus (loss modulus), and damping property (loss factor or tan δ) can be calculated.
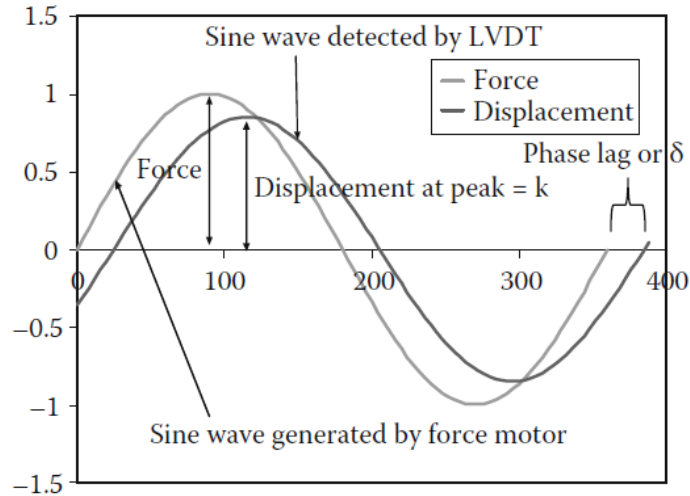
Figure 3-5 Applied sinusoidal force and resulting displacement [116]

Figure 11 shows typical storage modulus of amorphous thermoplastics as a function of temperature. A glass transition temperature – the transition from a glassy state into a rubbery state – is demonstrated as a sharp drop in storage modulus. Below this transition there are other transitions such as beta, gamma, and delta, which correspond with decreasing temperature to side chain movement, bending and stretching, and local motions, respectively. Unfortunately, these transitions are often hard to see in a storage modulus plot but can be detected through a loss modulus plot.
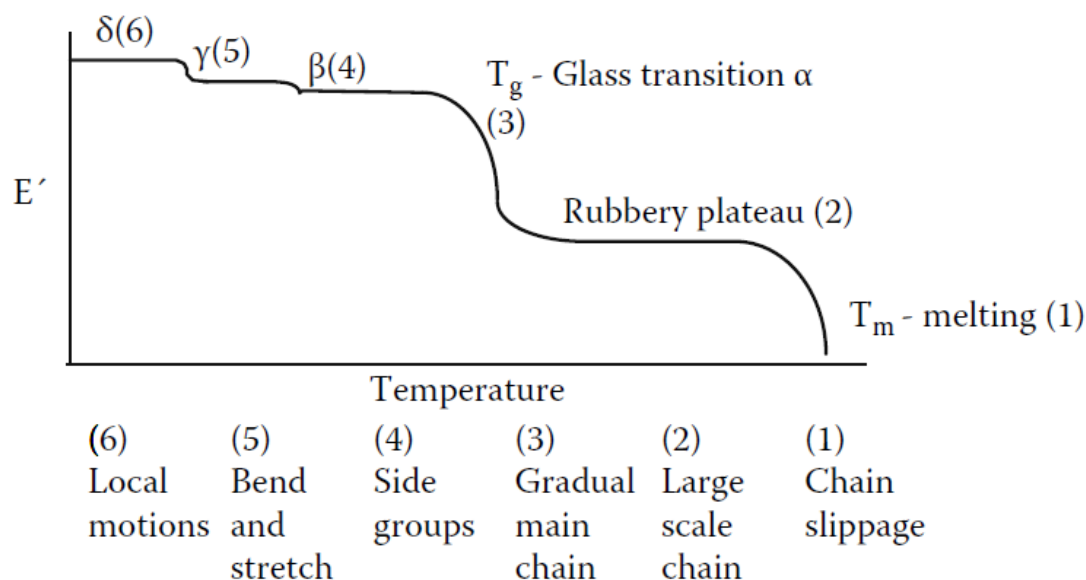
Figure 3-6 Various molecular relaxations demonstrated on a storage modulus, E', plot [116]

In this study, viscoelastic properties of the nanocomposites were studied using a dynamic mechanical analyser (DMA Q800, TA instruments). A sample was tested in a tensile mode at a frequency of 1 Hz. A strain amplitude was set to 0.1% to remain in the liner viscoelastic region and a heating rate was set to 5°C/min. Three samples were tested for each composition.

3.5   Thermogravimetric Analysis

Thermogravimetric analysis (TGA) is a characterization method that measure mass of a sample over a wide temperature range. TGA is commonly used to characterise thermal stability of a material. If a sample is thermally stable, there is no change in mass. When the sample begins to degrade, the mass decreases. A schematic of DMA set-up is represented in Figure 12.
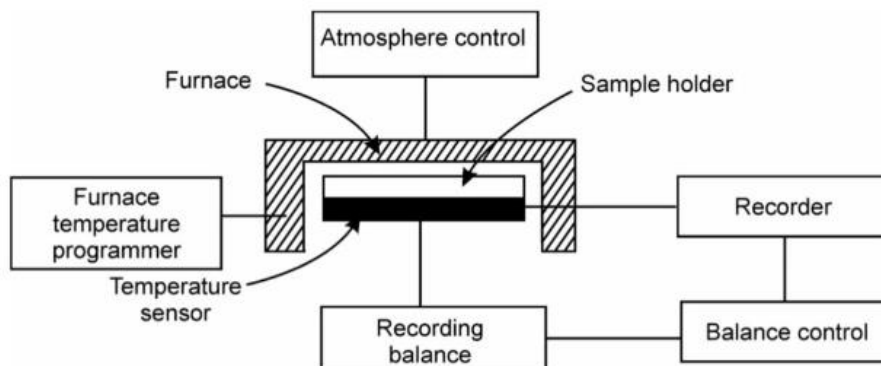
Figure 3-7 Schematic of DMA set-up [117]

A high-precision balance contains a small amount of a sample, which is surrounded by a furnace. A thermocouple is used to measure the temperature within the furnace. As the temperature is increased, the balance records the changes in weight. The environment can be controlled by using various types of gas such as inert gasses.

In this study, thermal stability of the nanocomposites was investigated using a thermogravimetric analyzer (TGA) (TGA Q50, TA Instruments). The mass of each sample was 8.5mg (±0.5 mg). A heating rate was set to 10°C/min. Purge gas was nitrogen and flow rates were set to 40 mL/min and 60 mL/min to the balance and sample areas, respectively. Three samples were tested for each composition.

The degree of conversion, α, of the sample was calculated by

$$\alpha = \left(\frac{M_o - M_t}{M_o - M_f}\right) \times 100 \tag{3.3}$$

where M_o, M_t, M_f are, respectively, the mass at the beginning of the decomposition profile, the corresponding mass at the decomposition level being calculated (e.g. mass when 20% decomposed), and the final mass after decomposition.

The activation energy for decomposition E_a was calculated from the TGA curves by the Horowitz-Metzger method [118]:

$$\ln[\ln(1 - \alpha)^{-1}] = \frac{E_a \theta}{R(T_{max})^2} \qquad (3.4)$$

where α is the degree of conversion, θ is (T - T_{max}) [K], T is the temperature [K], T_{max} is the temperature where the maximum rate of mass loss occurs [K], and R is the gas constant [8.31 J/(mol K)]. The activation energy for decomposition (slope) was determined by plotting $\ln[\ln(1 - \alpha)^{-1}]$ versus θ.

Chapter 4

4   Results and Discussion

## 4.1   Dispersion and Distribution of CNF in PMMA

The degrees of dispersion and distribution of CNFs in the PMMA matrix impact properties of the resulting composites. The ideal case assumes that when the CNF/PMMA/solvent was prepared, PMMA molecules were dissolved and extended in the solvent, and at the same time CNFs were homogeneously dispersed and distributed in the solvent. Furthermore, the dispersion and distribution of CNFs are maintained in the PMMA matrix during the evaporation process of the solvent. Different types of solvent have previously been used [97], [100]–[103], [105], [112]; however, there is no consensus on the ideal solvent for nanocellulose/PMMA nanocomposites. Acetone is a good candidate as a solvent to fabricate CNF/PMMA nanocomposites due to a good balance of the polarity for CNF and PMMA, easiness to evaporate from the resulting nanocomposites (i.e., low boiling temperature of 56°C), low health risk, and low cost.

Figure 13 shows a photograph of CNF/PMMA nanocomposite films with different CNF contents [0wt% (i.e., neat PMMA) 1.0wt%, 2.0wt%, 2.9wt%, and 4.8wt% CNF], while Figure 14 shows a photograph of CNF/Modified PMMA nanocomposite films with fixed CNF contents (0wt% CNF or 4.8wt% CNF) and different MAA contents in PMMA (0wt%, 0.5wt%, and 2.0wt%). Both figures indicate that transparent CNF/PMMA nanocomposite films with the various CNF contents and MAA contents in PMMA were successfully prepared through the solvent casting method with acetone.

Figure 15 shows a typical transmission electron micrograph of CNF/Modified PMMA nanocomposites with 4.8wt% CNF content and different MAA contents in PMMA (0wt%, 0.5wt%, and 2.0wt%). The image suggests that CNFs were well dispersed and distributed in all of the different PMMA matrices. Furthermore, CNFs were randomly oriented within the PMMA matrices. Therefore, the MAA content in PMMA had little effect on dispersion, distribution, and orientation of CNFs.
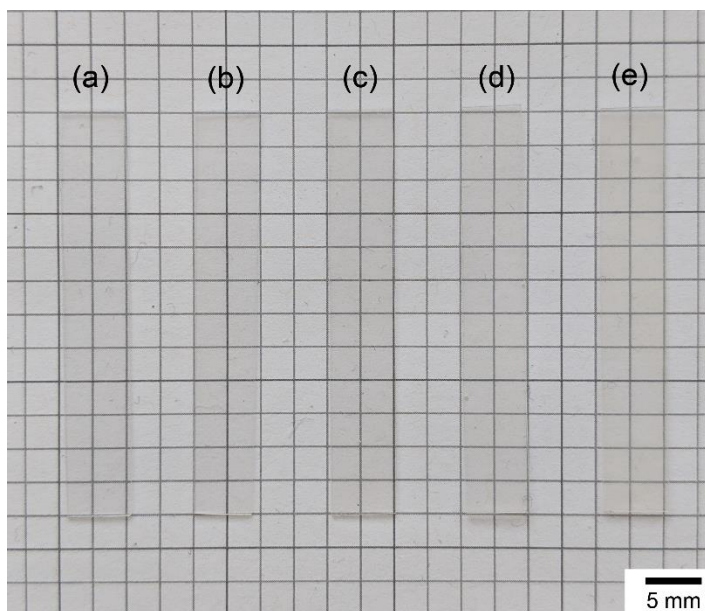
Figure 4-1 Photographs of CNF/PMMA nanocomposite films with different CNF contents: (a) 0wt% CNF (i.e., neat PMMA), (b) 1.0wt% CNF, (c) 2.0wt%, (d) 2.9wt% CNF, and (e) 4.8wt% CNF.
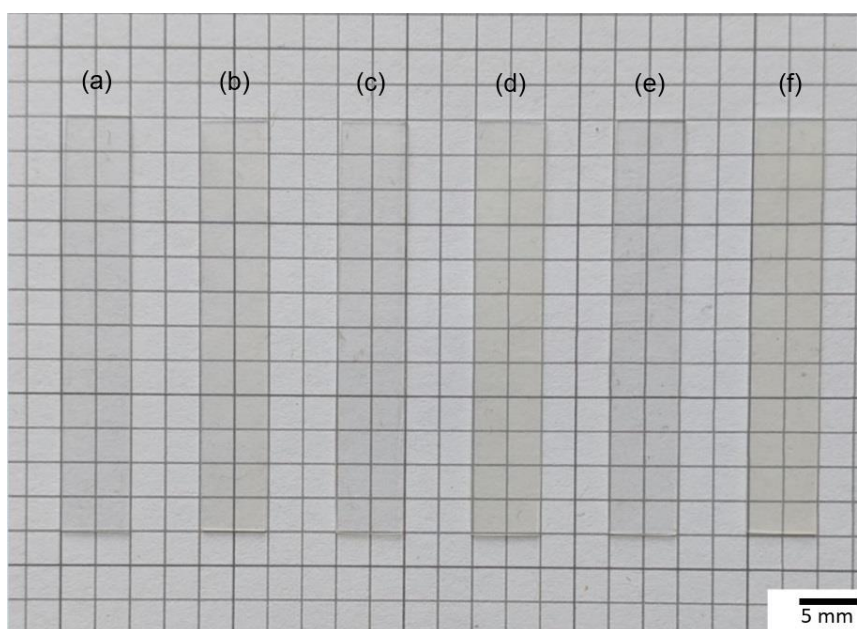
Figure 4-2 Photographs of CNF/Modified PMMA nanocomposite films with different MAA contents in PMMA: (a) 0%CNF/PMMA, (b) 4.8%CNF/PMMA, (c) 0%CNF/PMMA0.5, (d) 4.8%CNF/PMMA0.5, (e) 0%CNF/PMMA2.0, and (f) 4.8%CNF/PMMA2.0
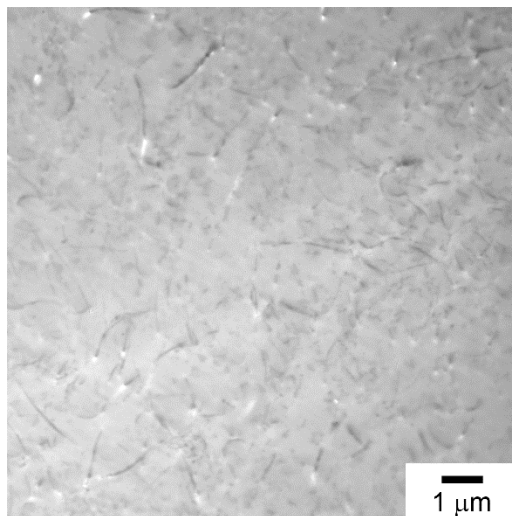
(a)

(b)

(c)

Figure 4-3 TEM image of (a) 4.8%CNF/PMMA, (b) 4.8%CNF/PMMA0.5, and (c) 4.8%CNF/PMMA2.0

4.2   Optical Property
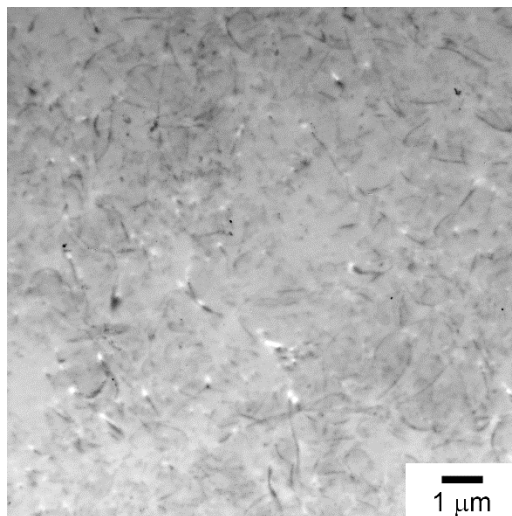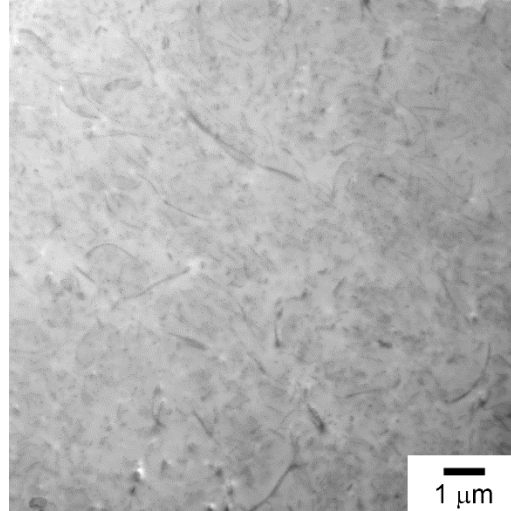
Although CNF is not a spherical particle, Rayleigh's law provides insight into key factors that affect transparency of nanocomposites [119], [120]:

$$\frac{I}{I_o} = exp\left[-\frac{3\phi_p x r^3}{4\lambda^4}\left(\frac{n_p}{n_m} - 1\right)\right] \qquad (4.1)$$

where I and I_o are, respectively, the intensity of the transmitted and incident light, Φ_p is the volume fraction of the particles, x is the optical path length, r is the radius of the spherical particles, λ is the wavelength of light, and n_p and n_m are, respectively, the refractive index of the particles and the matrix.

According to Rayleigh's law, transparency of CNF/PMMA nanocomposites depends on the following material parameters: refractive indices of CNF and PMMA, size of CNF, and volume fraction of CNF. The transparency of nanocomposites experiences no reduction from fibers if the refractive index of the fibers are identical to that of the matrix; however, CNF has a refractive index of 1.618 and 1.544 along the fiber and the transverse directions, respectively, while PMMA has a refractive index of 1.492 [8]. Although small,

the difference in refractive index between CNF and PMMA has an impact on transparency of the nanocomposites. Furthermore, when CNF agglomerates in the PMMA matrix and/or volume fraction of CNF increases, transparency of the nanocomposites decreases. In particular, agglomeration of CNF (i.e., large size of CNF) has a dramatic impact on the transparency.

Figure 16(a) shows UV-Vis transmittance versus wavelength for CNF/PMMA nanocomposites with different CNF contents. Transmittance decreased with decreasing wavelength for all the samples. Figure 16(b) shows how transmittance at selected wavelengths changed with the increase of CNF content. For each wavelength, transmittance decreased with increasing CNF content. However, larger reductions in transmittance were observed at lower wavelengths. There was a 15% reduction in transmittance at 700 nm between neat PMMA and 4.8wt% CNF/PMMA. An interesting phenomenon was observed below the visible light spectrum. UVA and UVB radiation exist between 320-400 nm and 290-320 nm, respectively, and have been a concern for many years due to the increased likelihood of skin cancer. At 300 nm and 350 nm, PMMA transmitted 73% and 78% of incident light, whereas 4.8wt% CNF/PMMA transmitted 21% and 37%, representing a remarkable 57% and 41% reduction in transmittance, respectively. In this regard, CNF/PMMA can provide a means to block a majority of UVA and UVB rays while remaining highly transparent with visible light.
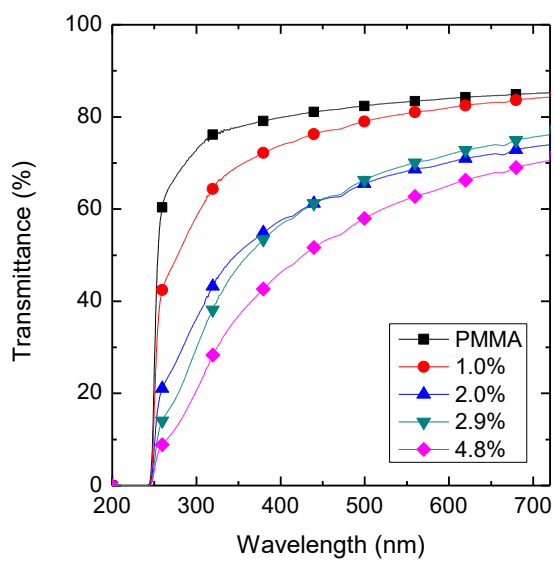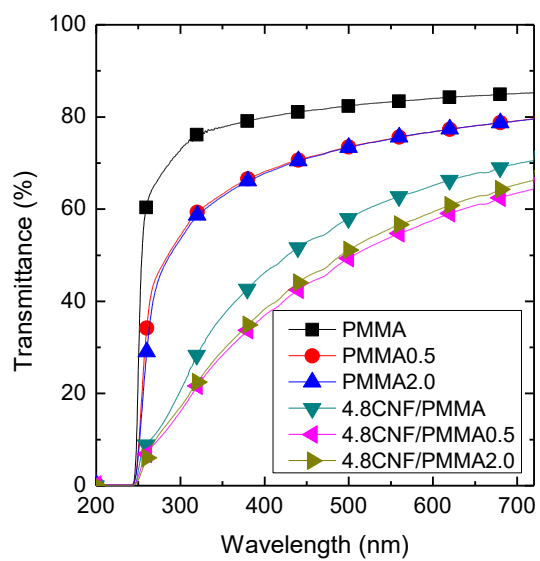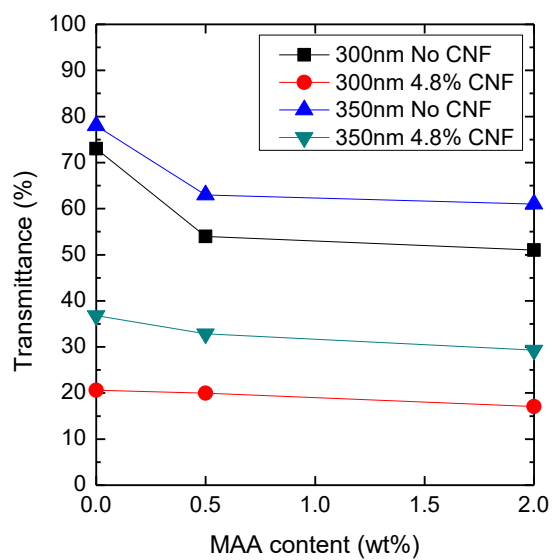
(a)
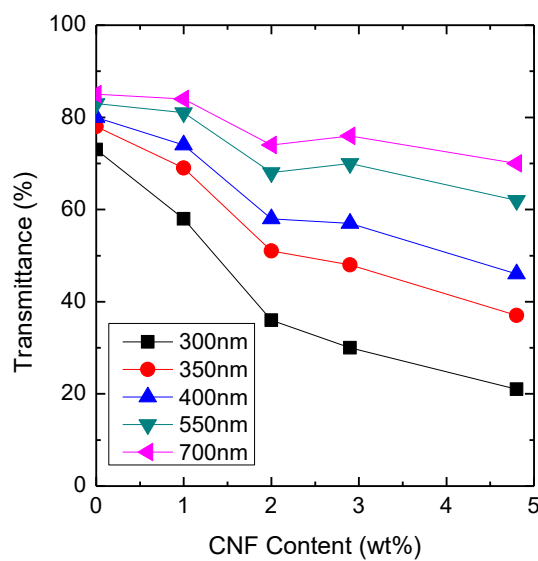
(b)

Figure 4-4 UV-Vis transmittance of CNF/PMMA nanocomposites as a function of (a) wavelength and (b) CNF content.

Figure 17(a) shows UV-Vis transmittance versus wavelength for CNF/Modified PMMA nanocomposite films with fixed CNF contents (0wt% CNF or 4.8wt% CNF) and different MAA contents in PMMA. Figure 17(b) and Figure 17(c) show how the transmittance in the UV region (300 nm and 350 nm) and in the visible light region (400 nm, 550 nm, and 700 nm), respectively, at selected wavelengths changes with an increase of MAA content. Similar effects of MAA content on transmittance were found in the UV and visible light regions. For the modified PMMA without CNF, addition of 0.5wt% MAA decreased transmittance, but further addition to 2.0wt% MAA decreased transmittance slightly further. When 4.8wt% CNF was added to the modified PMMA, a similar trend was observed to that of the modified PMMA without CNF (i.e., pure modified PMMA). That is, transmittance decreased from 0wt% to 0.5wt% MAA (4.8%CNF/PMMA to 4.8%CNF/PMMA0.5) and decreased slightly further from 0.5wt% MAA to 2.0wt% MAA (4.8%CNF/PMMA0.5 to 4.8%CNF/PMMA2.0). The results suggested that MAA content in PMMA had a minimal impact on the transmittance between 0.5wt% and 2.0wt%.

It should be noted that the addition of 4.8wt% CNF reduced transmittance of the modified PMMA more significantly at the UV region than the visible light region, which is useful to block UVA and UVB rays and keep high transparency of visible light. For example, at the wavelength of 700 nm, PMMA2.0 transmitted 78% of incident light and 4.8wt% CNF/PMMA2.0 transmitted 65%, representing a 13% reduction in transmittance. In contrast, at the wavelength of 300 nm and 350 nm, PMMA2.0 transmitted 51% and 61% of incident light, whereas 4.8wt% CNF/PMMA2.0 transmitted 17% and 29%, representing a 34% and 32% reduction in transmittance, respectively.

(a)

(b)
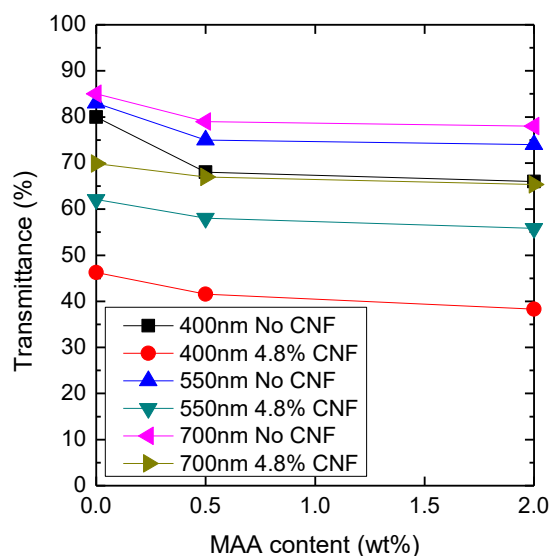
(c)

Figure 4-5 UV-Vis transmittance of CNF/Modified PMMA nanocomposites as a function of (a) wavelength, (b) MAA content in UV region, and (c) MAA content in visible light region.

4.3   Viscoelastic Property

Figure 18(a) shows typical DMA plots of storage modulus (E') versus temperature for CNF/PMMA nanocomposites with different CNF contents. Increasing temperature results in decreased E' for all the samples, resulting from the increase in molecular mobility provided by the thermal energy. It was found that the glass transition temperature (Tg), which was taken from the onset of the sigmoidal change of E', increased with the increase of CNF content (116.6°C for neat PMMA to 118.9°C for 4.8wt% CNF/PMMA), as shown in Table 8. The addition of CNF restricted chain mobility of PMMA, resulting in the glass transition shift to higher temperatures. Figure 18(b) shows how storage modulus at selected temperatures changed with the increase of CNF content. For each temperature, E' increased with the increase of CNF content. However, the addition of CNF was more effective at higher temperature. For example, the addition of 4.8wt% CNF increased E' of PMMA by 19% at 25°C and 30% at 100°C.
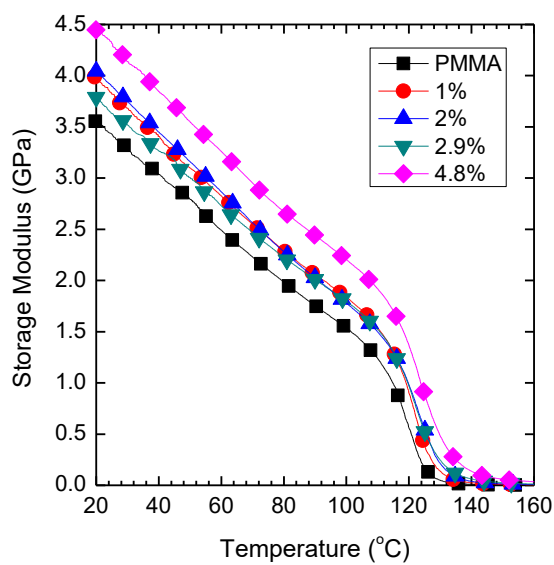
(a)
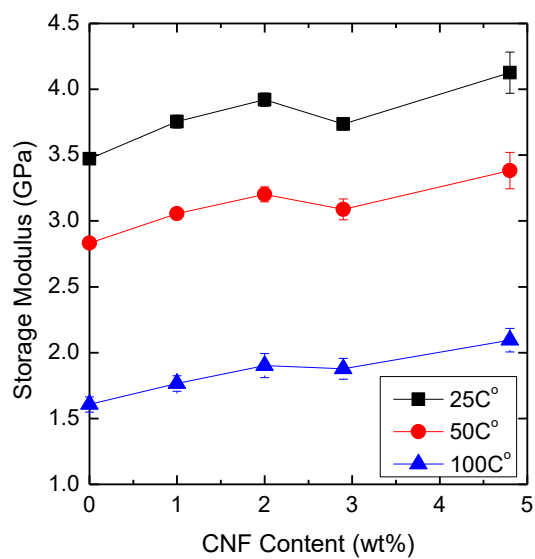
(b)

Figure 4-6 Storage modulus (E') of CNF/PMMA nanocomposites as a function of (a) temperature and (b) CNF content.

Table 4-1 Glass transition temperature and the coefficient *C* of CNF/PMMA nanocomposites with different CNF contents characterized from the DMA storage modulus curves. The numbers in the parenthesis are the standard deviations (n=3).

Sample	Glass Transition Temperature (^{o}C)	*C*
PMMA	116.6 (0.2)	
1.0% CNF/PMMA	117.0 (0.7)	0.507
2.0% CNF/PMMA	118.3 (0.2)	0.300
2.9% CNF/PMMA	117.5 (0.5)	0.215
4.8% CNF/PMMA	118.9 (0.5)	0.149

Figure 19(a) shows typical DMA plots of storage modulus (*E'*) versus temperature for CNF/Modified PMMA nanocomposites with fixed CNF contents (0wt% CNF or 4.8wt% CNF) and different MAA contents in PMMA. The figure demonstrates that *E'* increased slightly with the addition of 0.5% MAA, but decreased with further addition of 2.0% MAA. When 4.8wt% CNF was added to modified PMMA, *E'* was increased for all cases. On the other hand, T_g decreased with the increase of MAA content, as summarized in Table 9. It is speculated that addition of MAA may have interfered with cohesion and entanglement of PMMA molecules and thus decreased *Tg*. Further research into the causing mechanisms is required. When 4.8wt% CNF was added to modified PMMA, T_g increased for all cases. Figure 19(b) demonstrates how storage modulus at selected temperatures changed with the increase of MAA content. The addition of 4.8wt% CNF increased *E'* of PMMA, PMMA0.5, and PMMA2.0 by 19%, 16%, and 29% at 25°C, respectively, while increasing 30%, 23%, and 59% at 100°C. The results suggest that the addition of CNF was the most effective for PMMA with 2.0wt% MAA (PMMA2.0).
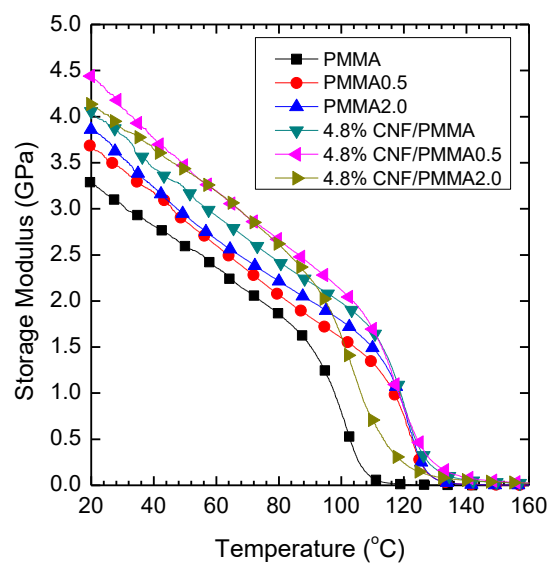
(a)
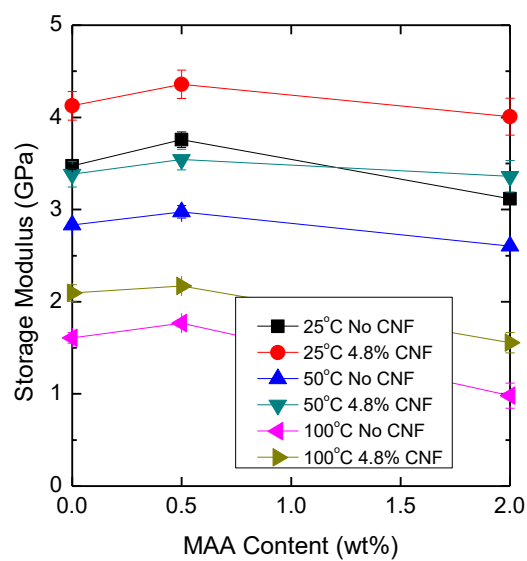
(b)

Figure 4-7 Storage modulus (E') of CNF/Modified PMMA nanocomposites as a function of (a) temperature and (b) MAA content in PMMA

As can be seen in Figure 19(a), the addition of CNF increased E' more effectively in the rubbery region (i.e., in the region above T_g) than in the glassy region (i.e., in the region below T_g). The coefficient C [121], [122] can be used as an index to quantify reinforcing effectiveness of fibers and is expressed as follows:

$$C = \frac{\left(E'_g/E'_r\right)_{composite}}{\left(E'_g/E'_r\right)_{resin}} \tag{4.2}$$

where E'_g and E'_r are the storage moduli in the glassy and rubbery regions at a specific shift in Tg.

The coefficient C is a relative measure of the decrease of storage modulus from the glassy state to the rubbery state. A low C value indicates an effective fiber to curb the decrease of E' after the glass transition. Table 8 shows C values obtained from E' in the glassy and rubbery regions taken 30°C away from Tg for different CNF content in PMMA. C decreased with the increase of CNF content. In the glassy state, the PMMA matrix is rigid with CNF contributing less to E' of the nanocomposites. On the other hand, in the rubbery state, the PMMA matrix is soft with CNF contributing more to E' of the nanocomposites.

Table 9 shows C values obtained from E' in the glassy and rubbery regions taken 30°C away from Tg for CNF/Modified PMMA nanocomposites. The results suggest that MAA may interact with CNF at higher temperatures (above T_g). The increased interfacial bonding between the modified PMMA and CNF may have decreased C. Further research into the causing mechanisms is required.

Table 4-2 Glass transition temperature and the coefficient *C* of CNF/Modified PMMA nanocomposites with different MAA contents in PMMA characterized from the DMA storage modulus curves. The numbers in the parenthesis are the standard deviations (n=3).

Sample	Glass Transition Temperature (ºC)	*C*
PMMA	116.6 (0.2)	
PMMA0.5	115.1 (1.0)	
PMMA2.0	98.7 (1.6)	
4.8% CNF/PMMA	118.9 (0.5)	0.149
4.8% CNF/PMMA0.5	115.2 (0.7)	0.090
4.8% CNF/PMMA2.0	100.4 (1.0)	0.074

Figure 20(a) shows typical DMA plots of loss modulus (E'') versus temperature for CNF/PMMA nanocomposites with different CNF contents. For all the samples, a peak was observed in the glass transition region. Also, E'' at near room temperature was higher than the peak value in the glass transition, which may be caused by the β relaxation of the PMMA matrix (i.e., pendent side chain mobility) [123]. E'' increased with the increase of CNF content due to the increased friction between CNF and PMMA molecules. In addition, the width of the loss modulus peak was broadened with the increase of CNF content. All the samples had a very similar onset temperature and slope up to the peak, which suggests that CNF had little effect on minimizing slippage leading up to the peak. However, a large widening occurred after the peak with increasing CNF content, which may have been caused by reduced mobility of PMMA region surrounding CNF (i.e., interphase region). Figure 20(b) shows how loss modulus at selected temperatures changed with the increase of CNF content. For each temperature, E'' increased with the increase of CNF content.

However, the influence of CNF addition was greater at higher temperatures. For example, the addition of 4.8wt% CNF increased E'' of PMMA by 13% at 25°C and 19% at 100°C.
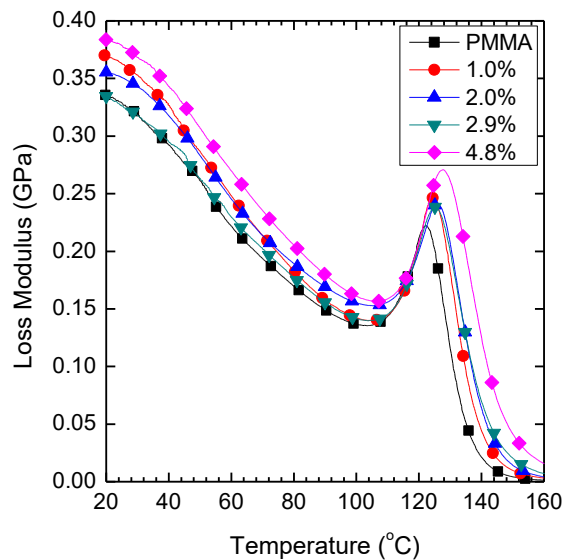
(a)
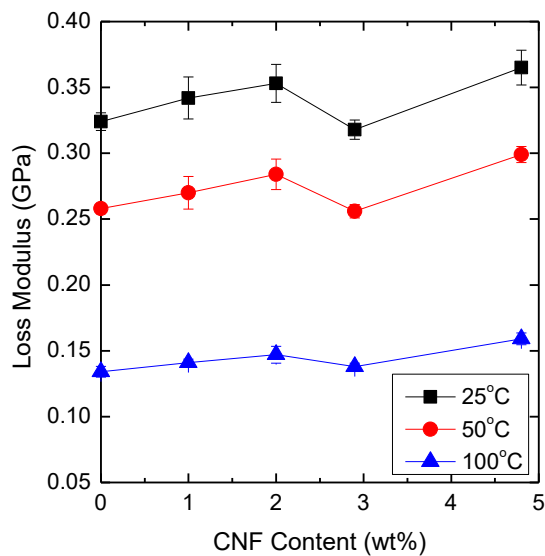
(b)

Figure 4-8 Loss modulus (E'') of CNF/PMMA nanocomposites as a function of (a) temperature and (b) CNF content.

Figure 21(a) shows representational DMA plots of loss modulus (E'') versus temperature for CNF/Modified PMMA nanocomposites with fixed CNF contents (0wt% CNF or 4.8wt% CNF) and different MAA contents in PMMA. The figure showed that E'' peak value increased with increasing MAA content. Furthermore, addition of 4.8wt% CNF increased E'' peak values for all the samples and broadened the width of the E'' peak.

Figure 21(b) shows how loss modulus at selected temperatures changes with increasing MAA content. The figure demonstrates that at the lower temperatures (25°C and 50°C), E'' increased slightly with the addition of 0.5% MAA, but decreased with further addition of 2.0% MAA and a similar effect on MAA content was observed for CNF/Modified PMMA nanocomposites. However, at the higher temperature (100°C), E'' did not decrease but increased with the addition of 2.0wt% MAA. This was because the testing temperature of 100°C was close to the glass transition temperatures of PMMA2.0 (98.7°C) and 4.8% CNF/PMMA2.0 (100.4 °C), where mobility of the modified PMMA molecules are increased, thus increasing friction between the modified PMMA molecules

The influence of CNF addition was greater at higher temperatures. The addition of 4.8wt% CNF in PMMA, PMMA0.5 and PMMA2.0 results in increases in loss modulus of 11%, 6%, and 19% at 25C, while increasing 16%, 23%, and 15% at 100C.
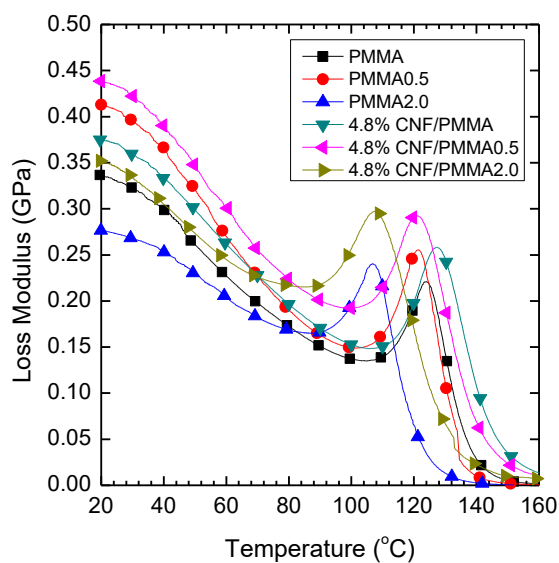
(a)

(b)

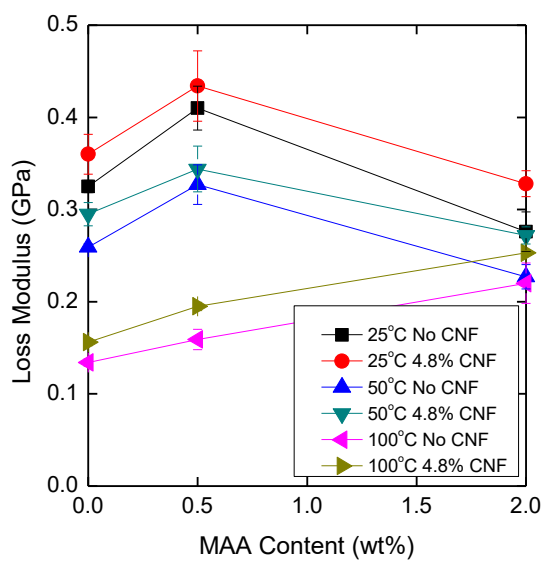**Figure 4-9 Loss modulus (E'') of CNF/Modified PMMA nanocomposites as a function of (a) temperature and (b) MAA content in PMMA.**

Figure 22(a) shows typical DMA plots of loss factor (tan δ) versus temperature for CNF/PMMA nanocomposites with different CNF contents. A peak can be observed in the glass transition region for all the samples. Figure 22(b) shows the peak value of loss factor versus CNF content. Tan δ peak decreased with the increase of CNF content: neat PMMA had a loss factor peak of 1.53 while 4.8wt% CNF/PMMA had 0.71. Therefore, the incorporation of CNF resulted in the change to a more elastic response around *Tg*.
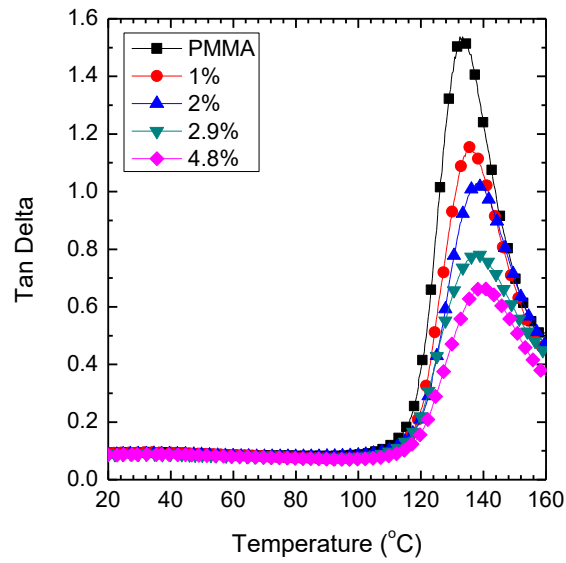
(a)
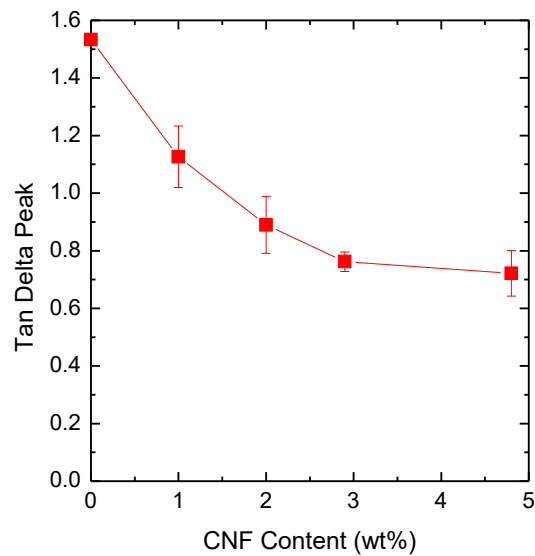
(b)

Figure 4-10 (a) Loss factor (tan δ) of CNF/PMMA nanocomposites with different CNF contents as a function of temperature and (b) loss factor (tan δ) peak of CNF/PMMA nanocomposites as a function of CNF content.

Figure 23(a) shows typical DMA plots of loss factor (tan δ) versus temperature for CNF/Modified PMMA nanocomposites with fixed CNF contents (0wt% CNF or 4.8wt% CNF) and different MAA contents in PMMA. A peak can be observed in the glass transition region for all the samples. Figure 23(b) shows the peak value of loss factor versus MAA content. For the modified PMMA without CNF, tan δ peak increased slightly with increasing MAA content. However, when 4.8wt% CNF was added to the modified PMMA, tan δ peak decreased with increasing MAA content, which may suggest that MAA in PMMA interacted with CNF.
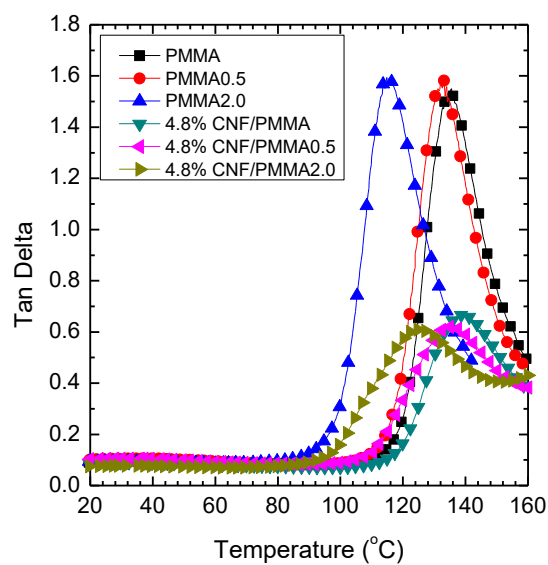
(a)
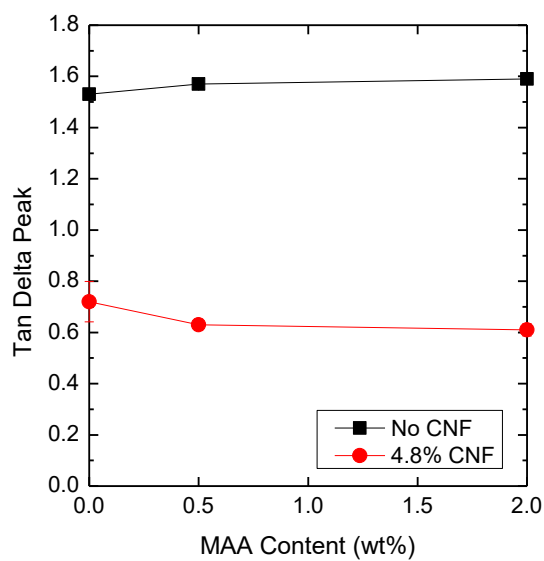
(b)

Figure 4-11 (a) Loss factor (tan δ) of CNF/Modified PMMA nanocomposites with different MAA contents in PMMA as a function of temperature and (b) loss factor (tan δ) peak of CNF/PMMA nanocomposites as a function of MAA content in PMMA.

4.4   Thermal Property

Figure 24(a) shows typical TGA plots of mass remaining versus temperature for CNF/PMMA nanocomposites with different CNF contents. The figure demonstrates that plots shifted to higher temperatures with the increase of CNF content. Figure 24(b) shows the temperature at 10% mass loss from room temperature versus CNF content. The temperature at 10% mass loss increased with the increase of CNF content and increased by 12.0°C from neat PMMA to 4.8wt% CNF/PMMA.
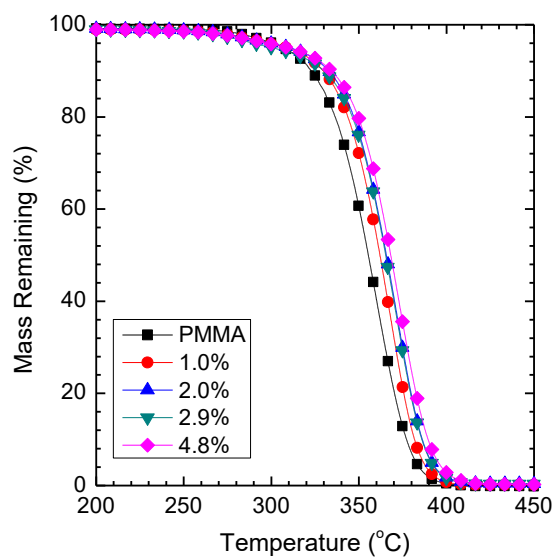
(a)
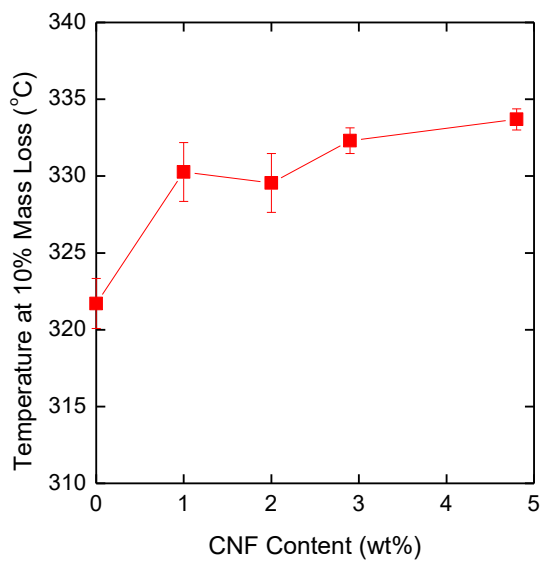
(b)

Figure 4-12 TGA curves of CNF/PMMA nanocomposites with different CNF contents and (b) temperature at 10% mass loss of CNF/PMMA nanocomposites as a function of CNF content.

Figure 25(a) shows representational TGA plots of mass remaining versus temperature for CNF/Modified PMMA nanocomposites with fixed CNF contents (0wt% CNF or 4.8wt% CNF) and different MAA contents in PMMA. The figure demonstrates that plots shifted to higher temperatures with the increase of MAA content in PMMA. Figure 25(b) shows the temperature at 10% mass loss from room temperature versus MAA content. The temperature at 10% mass loss increased with the increase of MAA content for both modified PMMA without and with CNF. For the modified PMMA without CNF, the temperature at 10% mass loss increased almost linearly with the increase of MAA content (322°C for PMMA, 327°C for PMMA0.5, and 335°C for PMMA2.0). When 4.8wt% CNF was added to the modified PMMA (334°C for 4.8%CNF/PMMA, 343°C for 4.8%CNF/PMMA0.5, and 350°C for 4.8%CNF/PMMA2.0). The addition of 4.8wt% CNF increased the temperature at 10% mass loss of PMMA, PMMA0.5, and PMMA2.0 almost constantly by 12°C, 16°C, and 15°C, respectively.
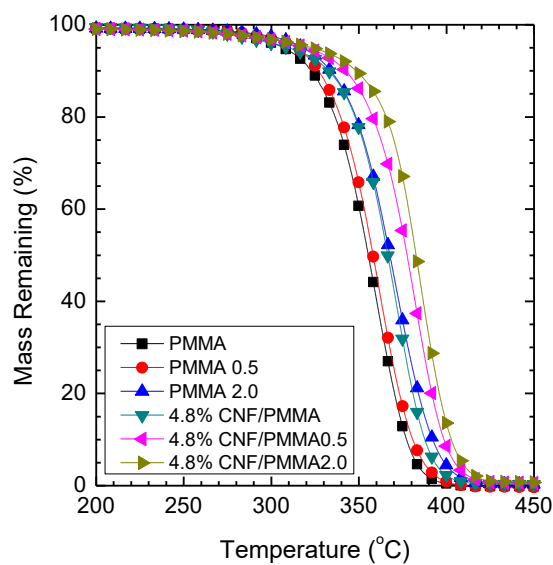
(a)
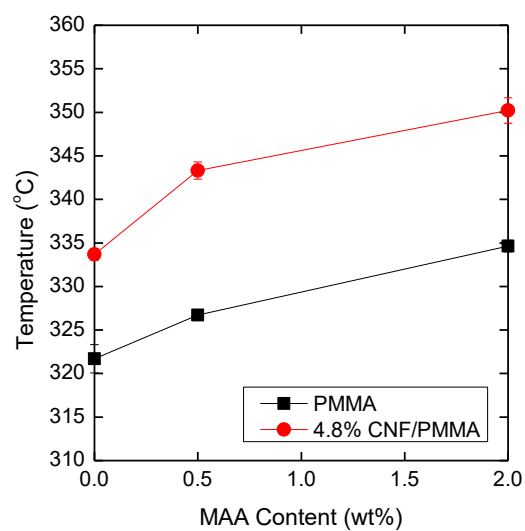
(b)

Figure 4-13 (a) TGA curves of CNF/Modified PMMA nanocomposites with different MAA contents in PMMA and (b) temperature at 10% mass loss of CNF/Modified PMMA nanocomposites as a function of MAA content in PMMA.

Figure 26(a) shows typical Horowitz-Metzger plots, that is, plots of $\ln[\ln(1-\alpha)^{-1}]]$ versus θ for CNF/PMMA nanocomposites with different CNF contents. The figure indicates that the trend lines for all the samples were almost linear. The slopes of trend lines were used to calculate activation energy. Figure 26(b) shows the activation energy versus CNF content. Activation energy increased from neat PMMA to 1.0wt% CNF/PMMA and remained roughly the same beyond 1.0wt% CNF loading (12% increase from neat PMMA to 4.8wt% CNF/PMMA).
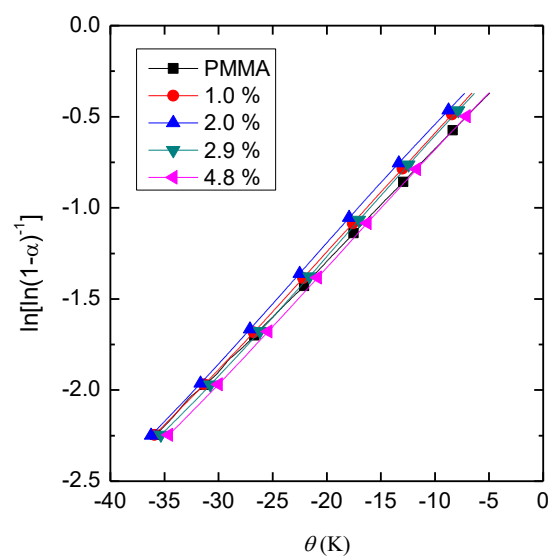
(a)
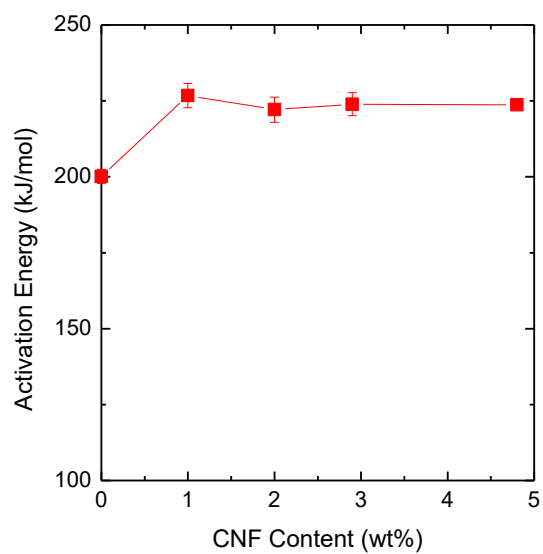
(b)

Figure 4-14 (a) Horowitz-Metzger plots of CNF/PMMA nanocomposites with different CNF contents and (b) activation energy of CNF/PMMA nanocomposites as a function of CNF content.

Figure 27(a) shows typical Horowitz-Metzger plots, that is, plots of $\ln[\ln(1-\alpha)^{-1}]]$ versus θ for CNF/Modified PMMA nanocomposites with fixed CNF contents (0wt% CNF or 4.8wt% CNF) and different MAA contents in PMMA. Similar to the results from the effects of CNF content, the figure indicates that the trend lines for all the samples were almost linear. Figure 27(b) shows the activation energy versus MAA content. Activation energy for decomposition of the modified PMMA without CNF increased slightly at 0.5wt% MAA content, while activation energy of the modified PMMA with 4.8wt% CNF showed an increase at 2.0wt% MAA content. The addition of 4.8wt% CNF increased activation energy of PMMA, PMMA0.5, and PMMA2.0 by 12%, 3% and 16%, respectively.
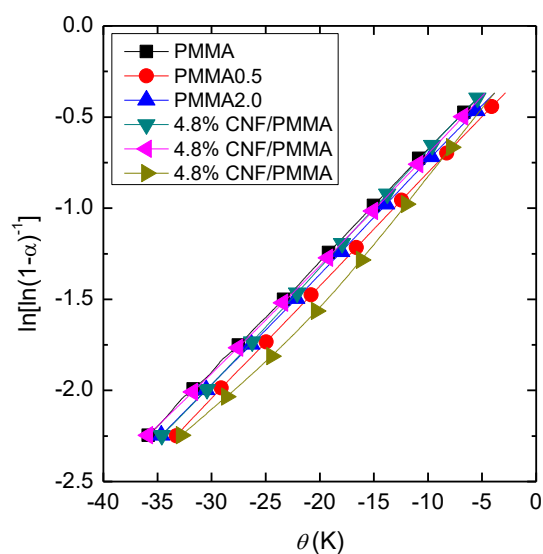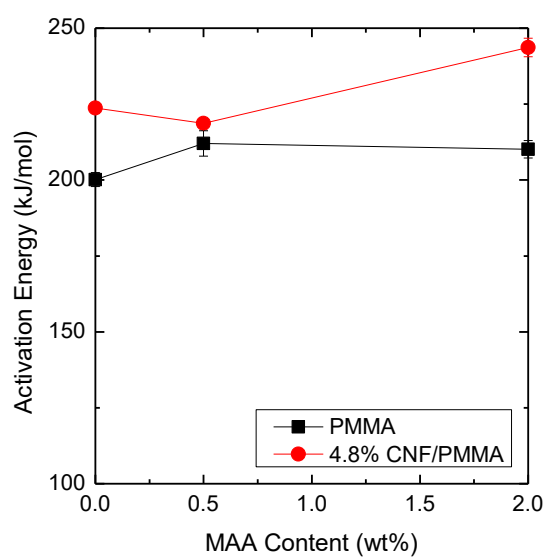
(a)

(b)

Figure 4-15 (a) Horowitz-Metzger plots of CNF/Modified PMMA nanocomposites with different MAA contents in PMMA and (b) activation energy of CNF/Modified PMMA nanocomposites as a function of MAA content in PMMA.

Chapter 5

5 Conclusions and Recommendations for Future Study

5.1 Conclusions

In recent years, nanocellulose has gained attention as a reinforcement in polymer nanocomposites mainly due to its low environmental impact and excellent physical properties [25], [31], [33], [35], [36]. Environmentally, nanocellulose is the most abundant polysaccharide on earth [16], [17], derived from many renewable resources (e.g., wood, cotton, bamboo, and bacteria) [33]–[35], and provides a natural, renewable, and readily available source of a fibrous reinforcement for nanocomposites. CNF is one of the two groups of nanocellulose, and includes both crystalline and amorphous regions and thus possess a higher aspect ratio. The main objective of this study was to develop transparent CNF/PMMA nanocomposites with good mechanical and thermal properties.

In this study, transparent CNF/PMMA, CNF/PMMA0.5, and CNF/PMMA2.0 nanocomposites were successfully prepared through a solvent casting method with acetone. TEM results showed that CNFs were well dispersed and distributed in the PMMA, PMMA0.5, and PMMA2.0 matrices.

UV-Vis results showed that transmittance of CNF/PMMA nanocomposites was reduced with increasing CNF content, decreasing 15% for 4.8wt% CNF samples in the visible light region at the wavelength of 700nm. However, a substantial decrease of transmittance in the UV region was observed, with a 57% and 41% reduction in UVA and UVB regions at the wavelengths of 300nm and 350nm, respectively. A similar trend was observed for the modified PMMA. The addition of 4.8wt% CNF decreased transmittance of PMMA2.0 by 13% in the visible light region. A substantial decrease was observed for PMMA2.0 in the UVA and UVB regions, with a 34% and 32% reduction.

DMA results showed that the addition of 4.8wt% CNF increased storage modulus of PMMA by 19% at 25°C and 30% at 100°C, glass transition temperature by 2.3°C, and loss modulus by 13% at 25°C and 19% at 100°C. On the other hand, the addition of 4.8wt%

CNF increased storage modulus of PMMA2.0 by 29% at 25°C and 59% at 100°C, glass transition temperature by 1.7°C, and loss modulus by 19% at 25°C and 15% at 100°C.

TGA results showed that the addition of 4.8wt% CNF increased the temperature at 10% mass loss by 12.0°C and activation energy by 12% for PMMA, while it increased the temperature at 10% mass loss by 15°C and activation energy by 16% for PMMA2.0.

In conclusion, highly transparent CNF/PMMA nanocomposites can be produced using a less hazardous and inexpensive solvent, acetone in a solvent casting method, and provide a means to enhance mechanical properties and thermal stability of PMMA and to block a majority of UVA and UVB rays. CNF/PMMA nanocomposites may be suitable for applications where good transparency, mechanical properties, and thermal properties are required, whereas CNF/PMMA0.5 and CNF/PMMA2.0 nanocomposites may be suitable for coating applications where adhesiveness as well as mechanical and thermal properties are more important. Therefore, the versatility of CNF/PMMA nanocomposites would have many potential applications.

5.2   Contributions

The past literature indicated that it has been challenging to improve both mechanical and thermal properties of PMMA by adding CNF while maintaining a high degree of transparency. In this study, the addition of CNF improved the properties of PMMA across the board (i.e., storage modulus, loss modulus, glass transition temperature, and thermal stability) without sacrificing their transparency. Furthermore, CNF was added to the modified PMMA and the addition of CNF improved the properties of the modified PMMA across the board without sacrificing their transparency, which has not been reported previously.

5.3   Recommendations for Future Study

The recommended future studies are described as follows:

(1)   CNF was used to increase physical properties of PMMA. There is another type of nanocellulose, cellulose nanocrystal (CNC), where the amorphous regions were

removed while the crystalline regions were remained. Because of its high crystallinity, CNC is expected to have higher Young's modulus and strength. However, CNF has shorter length and lower aspect ratio than CNF. It is interesting to compare optical, viscoelastic, and thermal properties of CNC/PMMA nanocomposites with CNF/PMMA nanocomposites, and to investigate effectiveness of these fibers.

(2)   In this study, CNFs were well dispersed and distributed in the PMMA matrix. However, PMMA is hydrophobic while CNF is hydrophilic in nature. Therefore, it is interesting to see how interfacial properties between CNF and PMMA affect optical, viscoelastic, and thermal properties of CNF/PMMA nanocomposites. The interfacial properties can be modified using surface modification of CNF or addition of coupling agents.

(3)   This study demonstrated that transparent CNF/PMMA nanocomposites can be produced through a solvent casting method and compression-molding. It will be beneficial to manufacture CNF/PMMA nanocomposites using more industry-friendly processes, such as melt-compounding and injection molding. However, CNF is easy to agglomerate and susceptible to thermal degradation, which will require in-depth study.

(4)   Numerical methods such as finite element analysis (FEA) can be used to predict mechanical and thermal properties of CNF/PMMA nanocomposites. This approach would also give better understanding of reinforcement and thermal stability mechanisms of CNF and would allow for simulation of mechanical and thermal properties when material parameters, such as matrix and fiber properties, fiber size, fiber geometry, and fiber volume fraction, are different.

References

[1]   N. P. Bansal and R. H. Doremus, *Handbook of Glass Properties*. Troy, New York: Academic Press, Inc., 1986.

[2]   I. I. Rubin, Ed., *Plastic Materials and Technology*. New York: John Wiley & Sons, Inc., 1990.

[3]   C. C. Ibeh, *Thermoplastic Materials: Properties, Manufacturing Methods, Applications*. Boca Raton: CRC Press Taylor & Francis Group, 2011.

[4]   E. Pawar, "A Review Article on Acrylic PMMA," *IOSR J. Mech. Civ. Eng.*, vol. 13, no. 2, pp. 1–4, 2016.

[5]   U. Ali, K. J. B. A. Karim, and N. A. Buang, "A Review of the Properties and Applications of Poly (Methyl Methacrylate) (PMMA)," *Polym. Rev.*, vol. 55, no. 4, pp. 678–705, 2015.

[6]   Market Research Report, "Polymethyl Methacrylate Market Size | PMMA Industry Report, 2025." 2017.

[7]   S.-W. Kuo, "Hydrogen-bonding in polymer blends," *J. Polym. Res.*, vol. 15, no. 6, pp. 459–486, Dec. 2008.

[8]   J. Brandrup, E. H. Immergut, and E. A. Grulke, Eds., *Polymer handbook*, 4th ed. New York, USA: John Wiley & Sons, Inc., 1999.

[9]   P. S. Malcom, *Polymer Chemistry: An Introduction. 3rd ed.* NY: Oxford University Press.

[10]   "Polymerization of PMMA," *Polymer Science Learning Center*. [Online]. Available: https://pslc.ws/macrog/pmma.htm. [Accessed: 20-Jun-2019].

[11]   L. Chang and E. M. Woo, "Tacticity effects on glass transition and phase behavior in binary blends of poly(methyl methacrylate)s of three different configurations," *Polym. Chem.*, vol. 1, no. 2, p. 198, 2010.

[12]   J. Karger-Kocsis, H. Mahmood, and A. Pegoretti, "Recent advances in fiber/matrix interphase engineering for polymer composites," *Prog. Mater. Sci.*, vol. 73, pp. 1–43, 2015.

[13]   V. K. Thakur and M. K. Thakur, "Processing and characterization of natural cellulose fibers/thermoset polymer composites," *Carbohydr. Polym.*, vol. 109, pp. 102–117, 2014.

[14]   H. T. Jitendra K. Pandey, Antonio N. Nakagaito, "Fabrication and Applications of Cellulose Nanoparticle-Based Polymer Composites," *Polym. Eng. Sci.*, pp. 1–6, 2013.

[15]   M. P. Coughlan, "Cellulases: Production, Properties and Applications," *Biochem. Soc. Trans.*, vol. 13, no. 13, pp. 405–6, 1985.

[16]   D. N.-S. Hon, "Cellulose: a random walk along its historical path," *Cellulose*, vol. 1, no. 1, pp. 1–25, Mar. 1994.

[17]   L. C. Duchesne and D. W. Larson, "Cellulose and the Evolution of Plant Life," *Am. Inst. Biol. Stud.*, vol. 39, no. 4, pp. 238–241, 2019.

[18]   M. A. S. Azizi Samir, F. Alloin, and A. Dufresne, "Review of recent research into cellulosic whiskers, their properties and their application in nanocomposite field," *Biomacromolecules*, vol. 6, no. 2, pp. 612–626, 2005.

[19]   D. Klemm, B. Heublein, H.-P. Fink, and A. Bohn, "Cellulose: Fascinating Biopolymer and Sustainable Raw Material," *Angew. Chemie Int. Ed.*, vol. 44, no. 22, pp. 3358–3393, May 2005.

[20]   G. Siqueira, J. Bras, and A. Dufresne, "Cellulosic bionanocomposites: A review of preparation, properties and applications," *Polymers (Basel).*, vol. 2, no. 4, pp. 728–765, 2010.

[21]   A. Chakrabarty and Y. Teramoto, "Recent advances in nanocellulose composites with polymers: A guide for choosing partners and how to incorporate them,"

Polymers (Basel)., vol. 10, no. 517, pp. 1–47, 2018.

[22] R. J. Moon, A. Martini, J. Nairn, J. Youngblood, A. Martini, and J. Nairn, "Cellulose nanomaterials review: structure, properties and nanocomposites," *Chem. Soc. Rev.*, no. 40, pp. 3941–3994, 2011.

[23] H. P. S. A. Khalil *et al.*, "Nanocellulose-Based Polymer Nanocomposite: Isolation, Characterization and Applications," in *Nanocellulose Polymer Nanocomposites*, Hoboken, NJ, USA: John Wiley & Sons, Inc., 2014, pp. 273–309.

[24] N. Lin, J. Huang, and A. Dufresne, "Preparation, properties and applications of polysaccharide nanocrystals in advanced functional nanomaterials: A review," *Nanoscale*, vol. 4, no. 11, pp. 3274–3294, 2012.

[25] K. Y. Lee, Y. Aitomäki, L. A. Berglund, K. Oksman, and A. Bismarck, "On the use of nanocellulose as reinforcement in polymer matrix composites," *Compos. Sci. Technol.*, vol. 105, pp. 15–27, 2014.

[26] M. E. Embuscado, "Purification and characterization of cellulose produced by Acetobacter xylinum," Purdue University, 1996.

[27] A. M. Maguire, "Bacterial cellulose-based medical devices," The University of Western Ontario, 1997.

[28] P. Dhar, U. Bhardwaj, A. Kumar, and V. Katiyar, "Cellulose Nanocrystals : A Potential Nanofiller for Food Packahing Applications." 2014.

[29] E. A. G. J. Brandrup, E. H. Immergut, *Polymer Handbook, 4th ed.* Wiley, New York, 1999.

[30] A. N. Nakagaito, S. Iwamoto, and H. Yano, "Bacterial cellulose: the ultimate nano-scalar cellulose morphology for the production of high-strength composites," *Appl. Phys. A Mater. Sci. Process.*, vol. 80, pp. 93–97, 2005.

[31] S. J. Eichhorn *et al.*, "Review: Current international research into cellulose

nanofibres and nanocomposites," *J. Mater. Sci.*, vol. 45, no. 1, pp. 1–33, 2010.

[32]   Y. Habibi, "Key advances in the chemical modification of nanocelluloses," *Chem. Soc. Rev.*, vol. 43, no. 5, pp. 1519–1542, 2014.

[33]   H. P. S. A. Khalil, A. H. Bhat, and A. F. I. Yusra, "Green composites from sustainable cellulose nanofibrils : A review," *Carbohydr. Polym.*, vol. 87, no. 2, pp. 963–979, 2012.

[34]   O. Nechyporchuk, M. N. Belgacem, and J. Bras, "Production of cellulose nanofibrils: A review of recent advances," *Ind. Crops Prod.*, vol. 93, pp. 2–25, 2016.

[35]   S. Mondal, "Preparation, properties and applications of nanocellulosic materials," *Carbohydr. Polym.*, vol. 163, pp. 301–316, 2017.

[36]   A. Dufresne, "Nanocellulose: A new ageless bionanomaterial," *Mater. Today*, vol. 16, no. 6, pp. 220–227, 2013.

[37]   K. Tashiro and M. Kobayashi, "Theoretical evaluation of three-dimensional elastic constants of native and regenerated celluloses: role of hydrogen bonds," *Polymer (Guildf).*, vol. 32, no. 8, pp. 1516–1526, 1991.

[38]   T. Nishino, K. Takano, and K. Nakamae, "Elastic Modulus of the Crystalline Regions of Cellulose Polymorphs," *J. Polym. Sci. Part B Polym. Phys.*, vol. 33, pp. 1647–1651, 1995.

[39]   F. T. Wallengberg, J. C. Watson, and H. Li, *ASM Handbook Vol. 21*. 2001.

[40]   V. Favier, G. R. Canova, S. C. Shrivastava, and J. Y. Cavaillé, "Mechanical percolation in cellulose whisker nanocomposites," *Polym. Eng. Sci.*, vol. 37, no. 10, pp. 1732–1739, 1997.

[41]   R. H. Marchessault, F. F. Morehead, and M. J. Koch, "Some Hydrodynamic Properties of Neutral As Related To Size and Shape 1," *J. Colloid Sci.*, vol. 344,

pp. 327–344, 1961.

[42]   Q. W. Haiyun Liu, Dagang Liu, Fei Yao, "Fabrication and properties of transparent polymethylmethacrylate/cellulose nanocrystals composites," *Bioresour. Technol. J.*, vol. 101, pp. 5685–5692, 2010.

[43]   A. Anžlovar, M. Huskić, and E. Žagar, "Modification of nanocrystalline cellulose for application as a reinforcing nanofiller in PMMA composites," *Cellulose*, vol. 23, no. 1, pp. 505–518, 2016.

[44]   M. Jonoobi, A. P. Mathew, and K. Oksman, "Producing low-cost cellulose nanofiber from sludge as new source of raw materials," *Ind. Crops Prod.*, vol. 40, no. 1, pp. 232–238, 2012.

[45]   M. Delgado-Aguilar, I. González, Q. Tarrés, M. Alcalà, M. À. Pèlach, and P. Mutjé, "Approaching a low-cost production of cellulose nanofibers for papermaking applications," *BioResources*, vol. 10, no. 3, pp. 5330–5344, 2015.

[46]   L. Berglund, M. Noël, Y. Aitomäki, T. Öman, and K. Oksman, "Production potential of cellulose nanofibers from industrial residues: Efficiency and nanofiber characteristics," *Ind. Crops Prod.*, vol. 92, pp. 84–92, 2016.

[47]   K. Uetani and H. Yano, "Nanofibrillation of wood pulp using a high-speed blender," *Biomacromolecules*, vol. 12, no. 2, pp. 348–353, 2011.

[48]   Y. Zhao, C. Moser, M. E. Lindström, G. Henriksson, and J. Li, "Cellulose Nanofibers from Softwood, Hardwood, and Tunicate: Preparation-Structure-Film Performance Interrelation," *ACS Appl. Mater. Interfaces*, vol. 9, no. 15, pp. 13508–13519, 2017.

[49]   M. Kottaisamy *et al.*, "Structure, morphology and thermal characteristics of banana nano fibers obtained by steam explosion," *Bioresour. Technol.*, vol. 102, no. 2, pp. 1988–1997, 2010.

[50]   S. Thomas, M. Kottaisamy, L. A. Pothan, S. F. de Souza, B. M. Cherian, and A. L.

Leão, "Isolation of nanocellulose from pineapple leaf fibres by steam explosion," *Carbohydr. Polym.*, vol. 81, no. 3, pp. 720–725, 2010.

[51]   K. Abe and H. Yano, "Comparison of the characteristics of cellulose microfibril aggregates isolated from fiber and parenchyma cells of Moso bamboo (Phyllostachys pubescens)," *Cellulose*, vol. 17, no. 2, pp. 271–277, 2010.

[52]   E. de Morais Teixeira, A. C. Corrêa, A. Manzoli, F. de Lima Leite, C. de Ribeiro Oliveira, and L. H. C. Mattoso, "Cellulose nanofibers from white and naturally colored cotton fibers," *Cellulose*, vol. 17, no. 3, pp. 595–606, 2010.

[53]   R. Ek, C. Gustafsson, A. Nutt, T. Iversen, and C. Nyström, "Cellulose powder from Cladophora sp. algae," *J. Mol. Recognit.*, vol. 11, no. 1–6, pp. 263–265, 1998.

[54]   T. Zimmermann, N. Bordeanu, and E. Strub, "Properties of nanofibrillated cellulose from different raw materials and its reinforcement potential," *Carbohydr. Polym.*, vol. 79, no. 4, pp. 1086–1093, 2010.

[55]   T. Zimmermann, E. Pöhler, and T. Geiger, "Cellulose fibrils for polymer reinforcement," *Adv. Eng. Mater.*, vol. 6, no. 9, pp. 754–761, 2004.

[56]   A. Dufresne, J. Cavaillé, and M. R. Vignon, "Mechanical behavior of sheets prepared from sugar beet cellulose microfibrils," *J. Appl. Polym. Sci.*, vol. 64, no. 6, pp. 1185–1194, 1997.

[57]   W. Stelte, C. Clemons, J. K. Holm, J. Ahrenfeldt, U. B. Henriksen, and A. R. Sanadi, "Fuel Pellets from Wheat Straw: The Effect of Lignin Glass Transition and Surface Waxes on Pelletizing Properties," *Bioenergy Res.*, vol. 5, no. 2, pp. 450–458, 2012.

[58]   A. Dufresne, *Nanocellulose: From Nature to High Performance Tailored Materials*. Walter de Gruyter GmbH & Co. KG, 2012.

[59]   S. Iwamoto, A. N. Nakagaito, and H. Yano, "Nano-fibrillation of pulp fibers for

the processing of transparent nanocomposites," *Appl. Phys. A Mater. Sci. Process.*, vol. 89, no. 2, pp. 461–466, 2007.

[60] A. Alemdar and M. Sain, "Isolation and characterization of nanofibers from agricultural residues - Wheat straw and soy hulls," *Bioresour. Technol.*, vol. 99, no. 6, pp. 1664–1671, 2008.

[61] Q. C. Cheng, S. Wang, and Q. Han, "Novel Process for Isolating Fibrils from Cellulose Fibers by High-Intensity Ultrasonication. II. Fibril Characterization," *J. Appl. Polym. Sci.*, vol. 115, no. 7, pp. 2756–2762, 2009.

[62] S. Wang and Q. Cheng, "A Novel Process to Isolate Fibrils from Cellulose Fibers by High-Intensity Ultrasonciation, Part 1: Process Optimization," *J. Appl. Polym. Sci.*, vol. 113, pp. 1270–1275, 2009.

[63] R. K. Johnson, A. Zink-Sharp, S. H. Renneckar, and W. G. Glasser, "A new bio-based nanocomposite: Fibrillated TEMPO-oxidized celluloses in hydroxypropylcellulose matrix," *Cellulose*, vol. 16, pp. 227–238, 2009.

[64] A. N. Nakagaito and H. Yano, "Novel high-strength biocomposites based on microfibrillated cellulose having nano-order-unit web-like network structure," *Appl. Phys. A Mater. Sci. Process.*, vol. 80, no. 1, pp. 155–159, 2005.

[65] J. Lu, T. Wang, and L. T. Drzal, "Preparation and properties of microfibrillated cellulose polyvinyl alcohol composite materials," *Compos. Part A Appl. Sci. Manuf.*, vol. 39, no. 5, pp. 738–746, 2008.

[66] A. N. Nakagaito and H. Yano, "The effect of morphological changes from pulp fiber towards nano-scale fibrillated cellulose on the mechanical properties of high-strength plant fiber based composites," *Appl. Phys. A Mater. Sci. Process.*, vol. 78, no. 4, pp. 547–552, 2004.

[67] A. Arora and G. W. Padua, "Review: Nanocomposites in food packaging," *J. Food Sci.*, vol. 75, no. 1, p. R43-, 2010.

[68] A. N. Frone, D. M. Panaitescu, D. D. Spataru, C. Radovici, R. Trusca, and R. Somoghi, "Preparation and characterization of PVA composites with cellulose nanofibers obtained by ultrasonication," *BioResources*, vol. 6, no. 1, pp. 487–512, 2011.

[69] D. N. S. Hon and N. Shiraishi, Eds., *Wood and Cellulosic Chemistry*, 2nd editio. New York: CRC Press Taylor & Francis Group.

[70] X. M. Dong, J. F. Revol, and D. G. Gray, "Effect of microcrystallite preparation conditions on the formation of colloid crystals of cellulose," *Cellulose*, vol. 5, no. 1, pp. 19–32, 1998.

[71] J. Araki, M. Wada, S. Kuga, and T. Okano, "Flow properties of microcrystalline cellulose suspension prepared by acid treatment of native cellulose," *Colloids Surfaces A Physicochem. Eng. Asp.*, vol. 142, no. 1, pp. 75–82, 1998.

[72] N. L. Garcia de Rodriguez, W. Thielemans, and A. Dufresne, "Sisal cellulose whiskers reinforced polyvinyl acetate nanocomposites," *Cellulose*, vol. 13, no. 3, pp. 261–270, 2006.

[73] D. Bondeson, A. Mathew, and K. Oksman, "Optimization of the isolation of nanocrystals from microcrystalline cellulose by acid hydrolysis," *Cellulose*, vol. 13, no. 2, pp. 171–180, 2006.

[74] J. Araki and S. Kuga, "Effect of Trace Electrolyte on Liquid Crystal Type of Cellulose Microcrystals," *Langmuir*, vol. 17, no. 15, pp. 4493–4496, 2001.

[75] W. P. Flauzino Neto *et al.*, "Mechanical properties of natural rubber nanocomposites reinforced with high aspect ratio cellulose nanocrystals isolated from soy hulls," *Carbohydr. Polym.*, vol. 153, pp. 143–152, 2016.

[76] J. George and S. N. Sabapathi, "Cellulose nanocrystals: Synthesis, functional properties, and applications," *Nanotechnol. Sci. Appl.*, vol. 8, pp. 45–54, 2015.

[77] S. J. Eichhorn, "Cellulose nanowhiskers: promising materials for advanced

applications," *Soft Matter*, vol. 7, no. 2, pp. 303–315, 2011.

[78] E. Mascheroni, R. Rampazzo, M. A. Ortenzi, G. Piva, S. Bonetti, and L. Piergiovanni, "Comparison of cellulose nanocrystals obtained by sulfuric acid hydrolysis and ammonium persulfate, to be used as coating on flexible food-packaging materials," *Cellulose*, vol. 23, no. 1, pp. 779–793, 2016.

[79] M. Yu *et al.*, "Preparation and Characterization Of Bamboo Nanocrystalline Cellulose," *Bio Resour.*, vol. 7, no. Copyright (C) 2015 American Chemical Society (ACS). All Rights Reserved., pp. 1802–1812, 2012.

[80] J. I. Morán, V. A. Alvarez, V. P. Cyras, and A. Vázquez, "Extraction of cellulose and preparation of nanocellulose from sisal fibers," *Cellulose*, vol. 15, no. 1, pp. 149–159, 2008.

[81] H. Yu, Z. Qin, B. Liang, N. Liu, Z. Zhou, and L. Chen, "Facile extraction of thermally stable cellulose nanocrystals with a high yield of 93% through hydrochloric acid hydrolysis under hydrothermal conditions," *J. Mater. Chem. A*, vol. 1, no. 12, pp. 3938–3944, 2013.

[82] I. Filpponen and D. S. Argyropoulos, "Regular Linking of Cellulose Nanocrystals via Click Chemistry : Synthesis and Formation of Cellulose Nanoplatelet Gels Regular Linking of Cellulose Nanocrystals via Click Chemistry : Synthesis and Formation of Cellulose Nanoplatelet Gels," no. MARCH 2010, pp. 1060–1066, 2015.

[83] T. Zhong, D. Liu, Q. Wu, K. Li, and P. R. Chang, "Starch composites reinforced by bamboo cellulosic crystals," *Bioresour. Technol.*, vol. 101, no. 7, pp. 2529–2536, 2009.

[84] M. A. Hubbe, O. J. Rojas, L. A. Lucia, and M. Sain, "Cellulosic Nanocomposites: A Review," *BioResources*, vol. 3, no. 3, pp. 929–980, 2009.

[85] Y. Habibi, L. A. Lucia, and O. J. Rojas, "Cellulose Nanocrystals : Chemistry, Self-Assembly, and Applications," *Chem. Rev.*, vol. 110, pp. 3479–3500, 2010.

[86] Roman. M and Winter. WT, "Effect of Sulfate Groups from Sulfuric Acid Hydrolysis on the Thermal Degradation Behavior of Bacterial Cellulose," *Biomacromolecules*, vol. 5, pp. 1671–1677, 2004.

[87] S. Sain *et al.*, "Synthesis and Characterization of PMMA-Cellulose Nanocomposites by In Situ Polymerization Technique," *J. Appl. Polym. Sci.*, vol. 126, pp. E127–E134, 2012.

[88] S. Camarero Espinosa, T. Kuhnt, E. J. Foster, and C. Weder, "Isolation of thermally stable cellulose nanocrystals by phosphoric acid hydrolysis," *Biomacromolecules*, vol. 14, no. 4, pp. 1223–1230, 2013.

[89] J. Araki, M. Wada, S. Kuga, and T. Okano, "Influence of surface charge on viscosity behavior of cellulose microcrystal suspension," *J. Wood Sci.*, vol. 45, no. 3, pp. 258–261, 1999.

[90] A. Nicharat, J. Sapkota, C. Weder, and E. J. Foster, "Melt processing of polyamide 12 and cellulose nanocrystals nanocomposites," *J. Appl. Polym. Sci.*, vol. 42752, pp. 1–10, 2015.

[91] K. Oksman *et al.*, "Review of the recent developments in cellulose nanocomposite processing," *Compos. Part A Appl. Sci. Manuf.*, vol. 83, pp. 2–18, 2016.

[92] H. Kargarzadeh *et al.*, "Recent developments on nanocellulose reinforced polymer nanocomposites: A review," *Polymer (Guildf).*, vol. 132, pp. 368–393, 2017.

[93] M. S. Salit, M. Jawaid, N. Bin, and E. Hoque, *Manufacturing of Natural Fibre Reinforced Polymer | Mohd Sapuan Salit | Springer*. Switzerland: Springer.

[94] J. Lu, P. Askeland, and L. T. Drzal, "Surface modification of microfibrillated cellulose for epoxy composite applications," *Polymer (Guildf).*, vol. 49, no. 5, pp. 1285–1296, 2008.

[95] M. A. S. Azizi Samir, F. Alloin, J. Y. Sanchez, N. El Kissi, and A. Dufresne, "Preparation of Cellulose Whiskers Reinforced Nanocomposites from an Organic

Medium Suspension," *Macromolecules*, vol. 37, no. 4, pp. 1386–1393, 2004.

[96]   D. Wang, J. Yu, J. Zhang, J. He, and J. Zhang, "Transparent bionanocomposites with improved properties from poly(propylene carbonate) (PPC) and cellulose nanowhiskers (CNWs)," *Compos. Sci. Technol.*, vol. 85, pp. 83–89, 2013.

[97]   E. Erbas Kiziltas, A. Kiziltas, S. C. Bollin, and D. J. Gardner, "Preparation and characterization of transparent PMMA-cellulose-based nanocomposites," *Carbohydr. Polym.*, vol. 127, pp. 381–389, 2015.

[98]   EPA, "N,N-Dimethylformamide 68-12-2," *United states Environ. Prot.*, no. 1, pp. 1–4, 2000.

[99]   G. Long, M. E. Meek, and M. Lewis, "Concise international chemical assessment document 31: N,N-dimethylformamide," *IPCS Concise Int. Chem. Assess. Doc.*, no. 31, pp. 1–56, 2001.

[100]   S. Sain, D. Ray, and A. Mukhopadhyay, "Improved Mechanical and Moisture Resistance Property of In Situ Polymerized Transparent PMMA/Cellulose Composites," *Polym. Compos.*, vol. 36, no. 9, pp. 1748–1758, 2015.

[101]   K. Littunen, U. Hippi, T. Saarinen, and J. Seppälä, "Network formation of nanofibrillated cellulose in solution blended poly(methyl methacrylate) composites," *Carbohydr. Polym.*, vol. 91, no. 1, pp. 183–190, 2013.

[102]   T. Huang, K. Kuboyama, H. Fukuzumi, and T. Ougizawa, "PMMA/TEMPO-oxidized cellulose nanofiber nanocomposite with improved mechanical properties, high transparency and tunable birefringence," *Cellulose*, vol. 25, no. 4, pp. 2393–2403, 2018.

[103]   S. Fujisawa, "Large specific surface area and rigid network of nanocellulose govern the thermal stability of polymers : Mechanisms of enhanced thermomechanical properties for nanocellulose / PMMA nanocomposite," *Mater. Today Commun.*, vol. 16, no. March, pp. 105–110, 2018.

[104] A. Boujemaoui, F. Ansari, and L. A. Berglund, "Nanostructural Effects in High Cellulose Content Thermoplastic Nanocomposites with a Covalently Grafted Cellulose–Poly(methyl methacrylate) Interface," *Biomacromolecules*, vol. 20, pp. 598–607, 2018.

[105] V. P. Anju and S. K. Narayanankutty, "Impact of Bis-(3-triethoxysilylpropyl)tetrasulphide on the properties of PMMA/Cellulose composite," *Polymer (Guildf).*, vol. 119, pp. 224–237, Jun. 2017.

[106] M. S. Huda, L. T. Drzal, A. K. Mohanty, and M. Misra, "Effect of fiber surface-treatments on the properties of laminated biocomposites from poly(lactic acid) (PLA) and kenaf fibers," *Compos. Sci. Technol.*, vol. 68, no. 2, pp. 424–432, 2008.

[107] M. Jonoobi, J. Harun, A. P. Mathew, and K. Oksman, "Mechanical properties of cellulose nanofiber (CNF) reinforced polylactic acid (PLA) prepared by twin screw extrusion," *Compos. Sci. Technol.*, vol. 70, no. 12, pp. 1742–1747, 2010.

[108] Y. Yoo, S. S. Kim, J. C. Won, K. Y. Choi, and J. H. Lee, "Enhancement of the thermal stability, mechanical properties and morphologies of recycled PVC/clay nanocomposites," *Polym. Bull.*, vol. 52, no. 5, pp. 373–380, 2004.

[109] C. Datta, D. Basu, and A. Banerjee, "Mechanical and dynamic mechanical properties of jute fibers-novolac-epoxy composite laminates," *J. Appl. Polym. Sci.*, vol. 85, no. 14, pp. 2800–2807, 2002.

[110] P. Tingaut, T. Zimmermann, and F. Lopez-Suevos, "Synthesis and characterization of bionanocomposites with tunable properties from poly(lactic acid) and acetylated microfibrillated cellulose," *Biomacromolecules*, vol. 11, no. 2, pp. 454–464, 2010.

[111] M. Tajvidi, R. H. Falk, and J. C. Hermanson, "Effect of natural fibers on thermal and mechanical properties of natural fiber polypropylene composites studied by dynamic mechanical analysis," *J. Appl. Polym. Sci.*, vol. 101, no. 6, pp. 4341–4349, 2006.

[112] M. Banerjee, S. Sain, A. Mukhopadhyay, S. Sengupta, T. Kar, and D. Ray,

"Surface treatment of cellulose fibers with methylmethacrylate for enhanced properties of in situ polymerized PMMA/cellulose composites," *J. Appl. Polym. Sci.*, vol. 131, no. 2, pp. 1–9, 2014.

[113] C. M. R. Facility, "Transmission Electron Microscopy," *University of Iowa*. [Online]. Available: https://cmrf.research.uiowa.edu/transmission-electron-microscopy. [Accessed: 20-Jun-2019].

[114] R. S. of Chemistry, "UV/visible spectroscopy." Royal Society of Chemistry, pp. 5–8.

[115] H.-H. Perkampus, *UV-vis Spectroscopy and Its Applications*. New York: Springer-Verlag, 1992.

[116] K. P. Menard, *Dynamic Mechanical Analysis*, vol. 2nd Editio. CRC Press, 2008.

[117] G. Forensics, "How Does Thermogravimetric Analysis Work ?" Gossman Forensics.

[118] H. H. Horowitz and G. Metzger, "A New Analysis of Thermogravimetric Traces," *Anal. Chem.*, vol. 35, no. 10, pp. 1464–1468, 1963.

[119] H. Althues, J. Henle, and S. Kaskel, "Functional inorganic nanofillers for transparent polymers," *Chem. Soc. Rev.*, vol. 36, no. 9, p. 1454, 2007.

[120] S. Li, M. Meng Lin, M. S. Toprak, D. K. Kim, and M. Muhammed, "Nanocomposites of polymer and inorganic nanoparticles for optical and magnetic applications," *Nano Rev.*, vol. 1, no. 0, pp. 1–19, Jan. 2010.

[121] L. A. Pothan, Z. Oommen, and S. Thomas, "Dynamic mechanical analysis of banana fiber reinforced polyester composites," *Compos. Sci. Technol.*, vol. 63, no. 2, pp. 283–293, Feb. 2003.

[122] S. C. A. Heitor Luiz Ornaghi, Jr., Alexandre Sonaglio Bolner, Rudinei Fiorio, Ademir Jose Zattera, "Mechanical and Dynamic Mechanical Analysis of Hybrid

Composites Molded by Resin Transfer Molding," *J. Appl. Polym. Sci.*, vol. 118, pp. 887–896, 2010.

[123] J. David S, "Dynamic mechanical analysis of polymeric systems of pharmaceutical and biomedical significance," *Int. J. Pharm.*, vol. 179, pp. 167–178, 1999.

Curriculum Vitae

Name:	Tyler Scott Michael Bennett

Post-secondary Education and Degrees:

Western University
London, Ontario, Canada
2016-2017 M.Eng Mechanical and Materials Engineering

Western University
London, Ontario, Canada
2012-2016 B.E.Sc Mechanical and Materials Engineering

The University of Western Ontario
London, Ontario, Canada
1995-1999 Ph.D.

Honours and Awards:

Western University
Dean's Honor List
2016, 2017

Related Work Experience

Teaching Assistant
Western University
ES1050 – Introduction to Engineering Design

Publications:

Bennett, T., Kuboki, T., and Sain, M. Effects of Cellulose Nanofiber Content on Optical, Viscoelastic, and Thermal Properties of Cellulose Nanofiber Reinforced Poly(methyl methacrylate). Annual Technical Conference 2019 of Society of Plastics Engineers, 18-21 March 2019, Detroit, Michigan, USA.